Geochemistry Geophysics Geosystems G3
AN ELECTRONIC JOURNAL OF THE EARTH SCIENCES
Published by AGU and the Geochemical Society

Article
Volume 10, Number 6
13 June 2009
Q06007, doi:10.1029/2008GC002295
ISSN: 1525-2027

Geomagnetic field for 0–3 ka: 1. New data sets for global modeling

F. Donadini
Institute of Geophysics and Planetary Physics, Scripps Institution of Oceanography, University of California, San Diego, 9500 Gilman Drive, La Jolla, California 92093-0225, USA (fdonadini@ucsd.edu)

M. Korte
Helmholtz-Zentrum Potsdam, Deutsches GeoForschungsZentrum, Telegrafenberg, D-14473 Potsdam, Germany (monika@gfz-potsdam.de)

C. G. Constable
Institute of Geophysics and Planetary Physics, Scripps Institution of Oceanography, University of California, San Diego, 9500 Gilman Drive, La Jolla, California 92093-0225, USA (cconstable@ucsd.edu)

[1] Paleomagnetic and archeomagnetic records are used in both regional and global studies of Earth's magnetic field. We present a description and assessment of five newly compiled data sets, also used in the companion paper by Korte et al. (2009) to produce a series of time-varying spherical harmonic models of the geomagnetic field for the last 3000 years. Data are drawn from our compilation of lake sediment records and from the online database, GEOMAGIA50v2. The five selections are available from the EarthRef Digital Archive at http://earthref.org/cgi-bin/erda.cgi?n=944. Data are grouped according to the source of material, and we conducted separate assessments of reliability for archeomagnetic artifacts and lava flows (the ARCH3k_dat data set) and for sediments (SED3k_dat). The overall number of data is 55% greater than in previous compilations. Constrained data sets were selected using different criteria for each group. Winnowing of archeological data was based on uncertainties supplied by the original data providers. The lake sediment data assessment relied on preassigned age uncertainties and one or more of the following: comparisons with archeomagnetic data from the same region, regional consistency among several lakes, and consistency with global archeomagnetic models. We discuss relative merits of a larger unconstrained data set or a smaller (possibly) more reliable one. The constrained data sets eliminate a priori up to 35% of the available data in each case and rely on potentially subjective assessments of data quality. Given the limited data available our analyses indicate that iterative rejection of a small number (1–1.5%) of outlying data during global field modeling is a preferable approach. Specific regional comparisons among the models and data support the conclusion that Korte et al.'s outlier-free CALS3k.3 model based on all available measurements from sediments and archeological artifacts currently provides the best global representation of the 0–3 ka field; the ARCH3k.1 model provides a better fit to the denser European archeomagnetic data and may be better in that region.

Components: 15,219 words, 12 figures, 9 tables.

Keywords: archeomagnetism; geomagnetic model; database.

Index Terms: 1503 Geomagnetism and Paleomagnetism: Archeomagnetism; 1560 Geomagnetism and Paleomagnetism: Time variations: secular and longer.

Received 24 October 2008; **Revised** 9 April 2009; **Accepted** 16 April 2009; **Published** 13 June 2009.

Donadini, F., M. Korte, and C. G. Constable (2009), Geomagnetic field for 0–3 ka: 1. New data sets for global modeling, *Geochem. Geophys. Geosyst.*, *10*, Q06007, doi:10.1029/2008GC002295.

1. Introduction

[2] Geomagnetic field data covering the Holocene period consist of measurements from natural rocks (e.g., recent lava flows), and from fired archeological artifacts (e.g., pottery, baked clays, bricks). Lake and some marine sediments with high accumulation rates provide another good source for directional data, and in some cases these also yield time series of relative intensity variations which can be calibrated to an absolute scale using model predictions to provide an appropriate scaling factor [*Korte and Constable*, 2006a]. These data have been used to study the variation of the geomagnetic field at centennial to millennial time scales which lie beyond the reach of direct observations. A review of such studies is provided by *Constable* [2007] and highlights several outstanding questions about field behavior. For example, the observed decay in magnetic field intensity during the past couple of centuries has triggered debate about whether or not Earth's magnetic field will undergo a reversal in the near future [*Hulot et al.*, 2002; *Constable and Korte*, 2006]. Another issue relates to changed perceptions about westward drift of the geomagnetic field: although it used to be generally accepted that the nondipolar part of the field drifted westward at a rate of about $0.3^\circ\ a^{-1}$ [*Merrill et al.*, 1996], analysis of historical data spanning the past 4 centuries suggests a more complicated view with westward drift prominent in the Indian Ocean/Atlantic hemisphere [*Jackson et al.*, 2000; *Bloxham et al.*, 1989], and more or less absent in the Pacific. On the longer term, *Dumberry and Finlay* [2007] and *Wardinski and Korte* [2008] analyze the secular variation using the CALS7K.2 model of *Korte and Constable* [2005] and show that episodes of eastward drift of the field also occur during the past 3000 and 7000 years, respectively. Drift direction in the Northern Hemisphere is related to changes in the two major high-latitude flux patches. The lower resolution of the model in equatorial regions and in the Southern Hemisphere does not allow for a detailed analysis there, and so there is no certainty about the existence of such episodes in these regions. The analysis of *Dumberry and Finlay* [2007] also finds a temporal correspondence between changes in flow direction in the model and the regional archeomagnetic jerks proposed by *Gallet et al.* [2003].

[3] It is well known that the magnetic field varies in both space and time, and its evolution has been studied both regionally and globally. The regional approach has been most effective in Europe where data density is relatively high and considering a region of interest enables evaluation of internal consistency of the data and study of the temporal evolution of the geomagnetic field. When several regions are examined, it is then also possible to investigate the spatial scale of field variations. There are several recent examples where this strategy has been used. For example, *Zananiri et al.* [2007] compiled a data set of archeomagnetic directions for the United Kingdom, relocated all the measurements to a common location, and studied the secular variation of the field using various approaches. They concluded that the optimum fitting of the data was achieved using the Bayesian approach described by *Lanos et al.* [2005] to develop regional secular variation curves. Similarly, *Tema et al.* [2006] and *Schnepp and Lanos* [2006] looked at the secular variations for Italy and Germany. For intensity data Virtual Axial Dipole Moments (VADMs) have been used to extend regional modeling to a global scale, and this strategy was used by *Genevey et al.* [2008] who studied the variation of the geomagnetic field intensity using a selected data set from archeological artifacts and lavas. A set of geographic regions were defined, VADMs within a region were calculated and averaged within overlapping temporal windows to provide regional temporal variation. Global VADM variations were determined from the average of all regions within each time window.

[4] Another approach consists of developing Spherical Harmonic (SH) models to represent the geomagnetic field in space and time during various geological eras [e.g., *Constable*, 2007, and references therein]. SH models have a long tradition of providing a mathematical description for the spatial structure of the field, and over the past 20 years it has become common to include a temporal parameterization in terms of cubic splines for the Gauss coefficients in the models. To build these models the time-varying coefficients of the geomagnetic field are derived directly from the observations. There are many solutions that would satisfy a particular data set, especially when the data are sparse and limited in accuracy, and so a regulariza-

tion technique is applied that favors models with minimal complexity and reasonable fit to the data. The resolution of the resulting model depends on how the complexity is measured, the distribution of measurements in time and space, and their perceived accuracy. The accuracy determines how observations are weighted in the modeling and what is a reasonable fit to the data, which ultimately controls the choice of the regularization parameter. Two widely used models of this type with quite different resolution are CALS7K.2 [*Korte and Constable*, 2005], describing the global geomagnetic field for the past 7000 years, and gufm1 [*Jackson et al.*, 2000] for 1590–1990 A.D. Each uses essentially the same measure of roughness or complexity, but the quality and coverage of the data are much better for the historical model.

[5] Regional models that demand consistent spatial variations have also been developed using various strategies. For example, *Pavon-Carrasco et al.* [2008] have used a variant of least squares spherical cap harmonic (SCH) modeling that closely fits European archeomagnetic data for the past 2000 years, and *Lodge and Holme* [2008] used CALS7K.2 as a background time-varying SH model that is updated by regularized inversion to provide an enhanced fit to five European Bayesian curves for the period 0–1900 A.D. These latter models are intended to be more accurate in a particular region (Europe in this case), and they have potential applications in archeomagnetic dating.

[6] The growing number of paleomagnetic data has encouraged researchers to create both regional and global compilations for the purpose of studying or modeling the features of the geomagnetic field in space and time [e.g., *Korte et al.*, 2005; *Donadini et al.*, 2006; *Zananiri et al.*, 2007; *Korhonen et al.*, 2008; *Genevey et al.*, 2008]. These compilations often include only the geomagnetic field measurements, the associated ages and locations; however, it has become obvious in recent years that other information like the material used, the method, or the dating technique adopted can be used as constraints to accept or reject a datum for a particular purpose and such information has in fact been compiled for some data sets [*Donadini et al.*, 2007; *Genevey et al.*, 2008]. The current work draws on and extends earlier efforts to generate two new compilations, one of paleomagnetic measurements from recent lake and rapidly deposited marine sediments records, and the second a more comprehensive collection of archeomagnetic and lava flow data including metadata, that has been used in producing version 2 of the online GEOMAGIA50 database (http://geomagia.ucsd.edu/). The major differences between these and earlier data collections are elaborated in the relevant parts of section 2 and the broader scope of GEOMAGIA50v2 is to be described in more detail elsewhere.

[7] We have drawn on these new compilations to construct five global data sets and study the effect of data selection based on different materials and specific reliability criteria. Each data set was then used to produce an SH model. For each data set we describe the quality of the data included and their distribution in space and time. The models generated are discussed in the context of evaluating the data and their regional consistency, but more details about their construction and resulting properties can be found in the companion paper by *Korte et al.* [2009]. We concentrate here on the past 3000 years because the temporal distribution of the archeomagnetic data only allows a thorough comparison and analysis for this period. A major goal of the current work is to assess whether global models with improved resolution are possible for the 0–3 ka time interval.

2. New 3k Data Set

[8] This section describes the newly assembled data collections for GEOMAGIA50v2 and the lake sediments that we have drawn on for our 5 data sets, with a particular emphasis on how they differ from earlier compilations.

[9] Table 1 outlines the origins and naming conventions used for the five different data sets and models for the 0–3 ka interval. As noted above we make a major distinction between archeological and lava flow data (designated ARCH3k) and sediment records (SED3k) and use this as the basis of the terminology for our data sets and models. When both kinds of source materials are involved we use CALS3k and we add "cst" when the specific constraints described in section 4 have been specified in the data selection. The data sets to be investigated are distinguished as follows: (1) all archeomagnetic observations (ARCH3k_dat), (2) all constrained archeomagnetic observations (ARCH3kcst_dat), (3) all lake sediments observations (SED3k_dat), (4) all archeomagnetic and lake sediments observations (CALS3k_dat), and (5) all constrained archeomagnetic and constrained lake sediments observations (CALS3kcst_dat).

[10] Table 2 shows the major sources of the data, along with the time span for the studies, and the

Table 1. Features of the Five Data Sets Used to Create the Models[a]

Features	LS Scaling	Data Set	Model
All AA	–	ARCH3k_dat[0, 1]	ARCH3k[0, 1]
All cst. AA	–	ARCH3kcst_dat[0, 1]	ARCH3k_cst[0, 1]
All LS	ARCH3k.1	SED3k_dat[0, 1]	SED3k[0, 1]
All AA and LS	ARCH3k.1	CALS3k.3_dat[0, 1]	CALS3k.3[0, 1]
All cst. AA and LS	ARCH3k.1/AA	CALS3kcst_dat[0, 1]	CALS3k_cst[0, 1]

[a] The LS scaling column gives the relative paleointensity calibration method: by means of the ARCH3k model or also using the values from archeological artifacts (AA, see section 2.2). The data set name represents the name of the file where all observations are stored, whereas the model name shows the name of each model. The numbers given in square brackets indicate the version of each file or model and relate to the files/models prior to [0] or after [1] rejection of outliers.

information available. This list is not a comprehensive catalog of regional or even global data compilation efforts, since many such data collections have subsequently been incorporated into larger activities like CALS7K or GEOMAGIA50v1. However, it is now the case that all the archeomagnetic and volcanic data from the appropriate age intervals in all the compilations listed has been included in GEOMAGIA50v2, after careful checks to avoid data duplication. In GEOMAGIA50v2 individual data are flagged so that it is possible to determine which data belong in each compilation. To our knowledge GEOMAGIA50v2 is the first compilation created with all the geomagnetic field directions, intensities, and additional metadata. The sediment data were compiled from each of the individually published studies, and are described in detail in section 2.2. Part of the CALS7K.2 data set was used to create the CALS3K.2 model, which spans the same interval as the models produced here. In Figure 1 we show sources of data from the past 3000 years that were not in CALS7K.2. About 10600 new data are available.

2.1. Archeological Artifacts and Lavas

[11] *Donadini et al.* [2006] and *Korhonen et al.* [2008] compiled and described a user friendly database, named GEOMAGIA, that included all available geomagnetic field intensities from igneous rocks and archeological artifacts covering the past

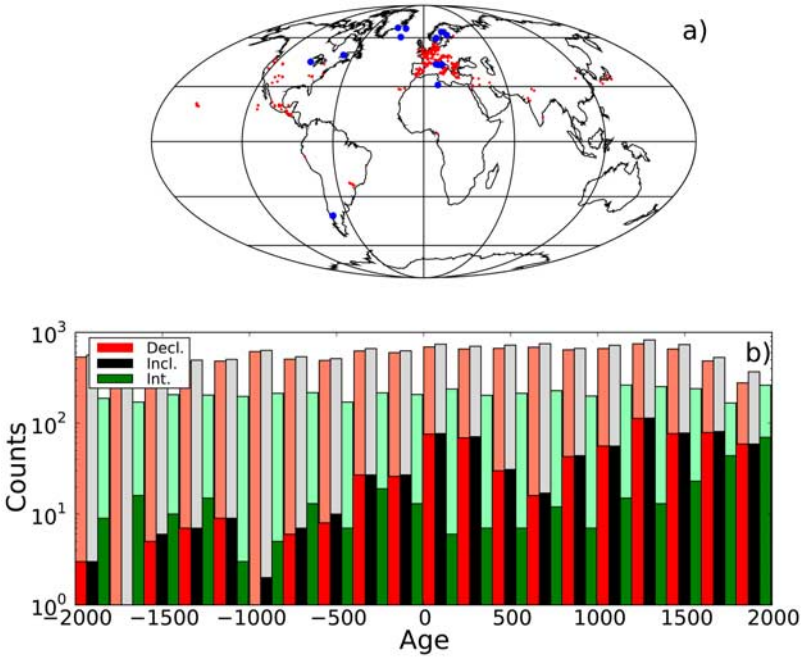

Figure 1. (a) New data, not available from CALS3k.2 and CALS7K.2 [*Korte and Constable*, 2005], covering the past 4000 years. Red (blue) circles show archeological artifacts (lake sediments); notice that a few lakes overlap and so are not distinguishable in the map. In total, about 10600 new data are included in the new data set. (b) Histogram showing the distribution of components over the past 4000 years in 200 year bins. Dark colors indicate archeological artifacts, whereas pastel colors indicate lake sediments. Notice the logarithmic scale.

Table 2. Various Existing Compilations and Their Time Span, Coverage, Geomagnetic Field Parameters Included, and Metadata[a]

Compilation Name	Time Span	Coverage	GMP	MD	Reference
ArcheoInt	Holocene	global	F	yes	*Genevey et al.* [2008]
GEOMAGIA50v1	past 50000 years	global	F	yes	*Donadini et al.* [2006]
ARCHEO00	Holocene	global	D, I	no	D. H. Tarling (personal communication, 2000)
PINT	Precambrian to present	global	F	yes	
CALS7K	past 7000 years	global	D, I, F	no	*Korte et al.* [2005]
Bulgaria	past 8000 years	Bulgaria	D, I, F	yes	*Kovacheva et al.* [2009]
Germany	past 8000 years	Germany	D, I	no	*Schnepp and Lanos* [2006]
Hungary	past 2000 years	Hungary	D, I	no	*Márton and Ferencz* [2006]
Italy	past 7000 years	Italy	D, I	no	*Tema et al.* [2006]
Spain	past 2000 years	Spain	D, I	no	*Gomez-Paccard et al.* [2006]
UK	past 5000 years	United Kingdom	D, I	no	*Zananiri et al.* [2007]
GEOMAGIA50v2	past 50000 years	global	D, I, F	yes	this study

[a] Geomagnetic field parameters (GMP) are defined as declinations (D), inclinations (I), or intensities (F). MD, metadata.

50,000 years. The GEOMAGIA database has now been updated and extended to include directional data. The upgraded database, designated GEOMAGIA50v2, is hosted online at the University of California, San Diego (http://geomagia.ucsd.edu/), and the Web site can be interrogated directly for the references to the studies included. The subsets of data used in this 0–3 ka study can be downloaded from the EarthRef digital archive at Earthref.org.

[12] The base from which we started was the original GEOMAGIA (GEOMAGIA50v1) and directions available from the CALS7K compilation of *Korte et al.* [2005]: this latter included the IAGA archeomagnetic directional database ARCHEO00 (http://www.ngdc.noaa.gov/geomag/paleo.shtml) assembled by D. Tarling. We updated the existing collection with newly gathered and previously unavailable data published up to fall 2007, and highlight some of the major new contributions here. A number of recent studies of the directional variation of the geomagnetic field in Europe became available within the AARCH programme (http://www.meteo.be/CPG/aarch.net/index.html), and so a thorough comparison was carried out in order to complete GEOMAGIA whilst avoiding duplications. The aim of the AARCH studies was to put together homogeneous regional data sets for archeomagnetic dating purposes, and in general the data sets were analyzed using the Bayesian approach described by *Lanos et al.* [2005] to create master curves with uncertainty estimates for particular regions. Data sets were compiled for United Kingdom [*Zananiri et al.*, 2007], Italy [*Tema et al.*, 2006], Germany [*Schnepp and Lanos*, 2006], Spain [*Gomez-Paccard et al.*, 2006], and Hungary [*Márton and Ferencz*, 2006]. Part of the work by *Tema et al.* [2006] relies on a previous compilation of *Lanza et al.* [2005].

[13] For paleointensities an important contribution is the ArcheoInt compilation of *Genevey et al.* [2008], which includes all archeointensity determinations of the past ten millennia, and additional information concerning the setup of each study. This particular study was used for comparison and cross checking of the intensity values available in GEOMAGIA50v1. Finally, the Bulgarian database [e.g., *Kovacheva*, 1997; *Kovacheva et al.*, 2009] has been revised within a common project with Mary Kovacheva of the Bulgarian Academy of Sciences in Sofia. Some mean values from old data have been recalculated after the addition of new measurements, and several ^{14}C ages were recalibrated using the Oxcal software of *Ramsey* [1994]. In total, 11 existing compilations have been cross checked and incorporated into the new GEOMAGIA50v2 (Table 2).

[14] As we indicated earlier our target is to produce a data set suitable for revised studies of the 0–3 ka geomagnetic field and to achieve a better resolution compared to previous available models. In the CALS7K.2 model studies, *Korte and Constable* [2006b] noted some inaccuracies in model predictions for the most recent times, which they attributed to end effects associated with the spline temporal basis. They supposed that similar unverifiable effects might occur in the earliest part of the record. To avoid such effects near 1000 B.C., the starting point of the models to be produced in this study, it was decided to include the observations back to 2000 B.C. in the data sets, and use the data between 2000 B.C. and 1000 B.C. to constrain the early part of the new model. For this reason, the data distri-

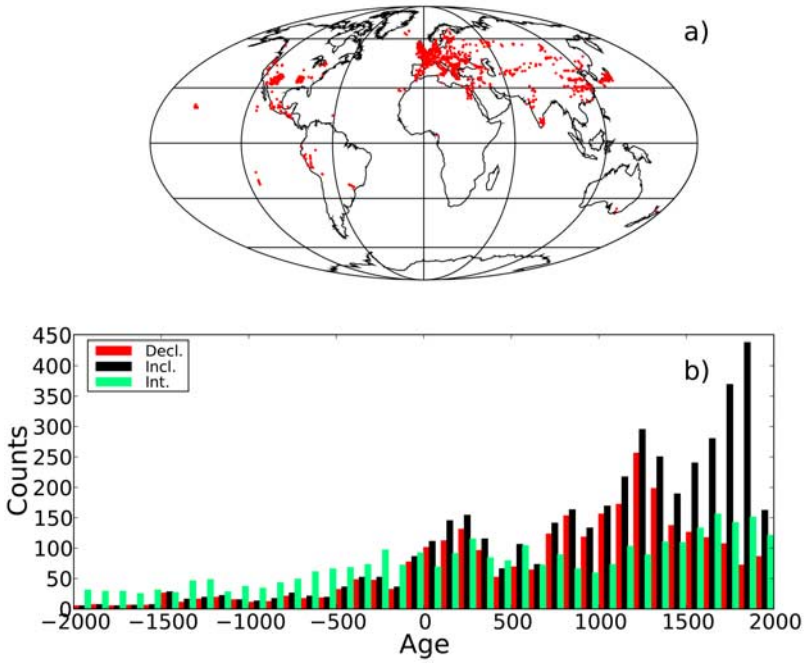

Figure 2. (a) The distribution of the archeological artifacts and lavas on the globe (ARCH3k_dat0), covering the past 4000 years. (b) Temporal distribution of declinations, inclinations, and intensities during the past 4000 years. Data are grouped in 100 year bins.

butions shown in Figures 1–3 include data for the past 4000 years. Figure 2a shows the spatial distribution of archeological and lava flow data and Figure 2b shows the temporal distribution over the past 4000 years for each component, in 100 year bins. The data are more numerous for recent time intervals, and in the Northern Hemisphere are most heavily concentrated in Europe and next most in Asia. The Southern Hemisphere is very poorly sampled, and contains less than 3% of the data. While the number of paleointensities for the past 4000 years is fairly constant (25–50 per bin), the number of directional data is more variable, with inclinations dominating in the most recent epochs and the number of data for both directional components decreasing rather sharply as we go back in time (Figure 2b). For the past 3000 (4000) years the GEOMAGIA50v2 database contains 2671 (2877) declinations, 4174 (4304) inclinations, and 2670 (3001) intensities. In the early part of the Holocene period, measurements from archeological artifacts rapidly decrease in number. Their relative abundance during the past 3000–4000 years motivates our choice of 1000 B.C. to 1990 A.D. as the time interval for this revised modeling. The entire Holocene data set would consist of 3427 declinations, 4929 inclinations, and 3905 intensities, only 30% more than in the 0–3 ka interval.

[15] Notice that ten data have not been included in the data set because of internal inconsistencies. In two cases the inclination was significantly shallower for the given latitude (data number 1817 and 2156), whereas in the other eight cases the scatter in declination was large enough to cause spurious departures in the model. In all 10 cases the whole measurement was rejected. Table 3 shows the identities of these entries in the GEOMAGIA50v2 database, as well as the site name of the archeological place, its latitude and longitude; the age, declination, inclination, and reference to the study.

2.2. Sediment Directional Data and Paleointensity Calibration

[16] The compilation of lake and rapidly accumulated marine sediments that make up SED12k is listed in Table 4 in terms of lake name, its abbreviation (used for example in the public files), the region where the lake is located, its latitude and longitude, as well as the age range covered by the core. The column labeled N also reports the number of data for each component (declination/inclination/intensity); whereas N_{REJ} shows the number rejected (declination/inclination/intensity) on the basis of the constrained data selection described in section 4 (Cst. column). Finally, the dating method used is also listed. The existing compilation of lake (and a

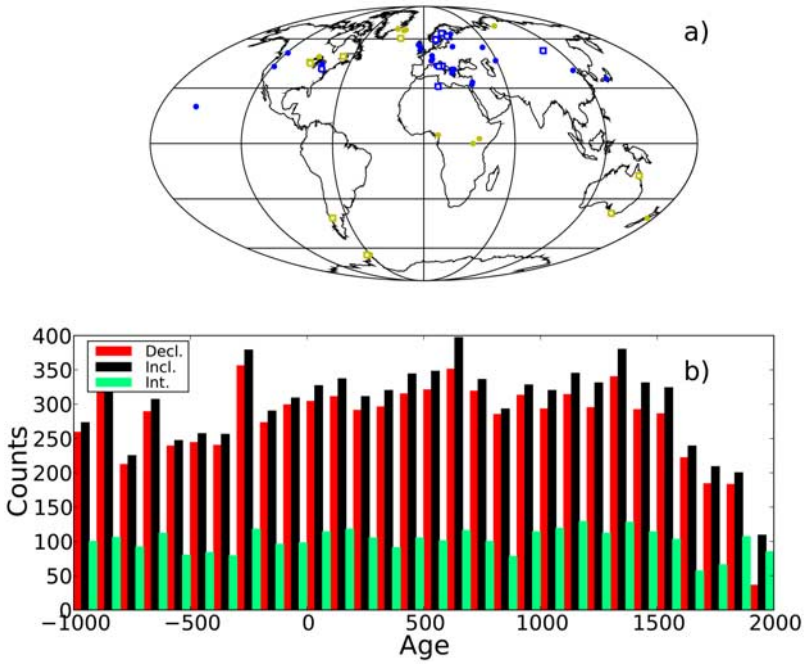

Figure 3. (a) The distribution of the lake sediments having archeological artifacts lying in a 1000 km radius from the center of the lake (blue) and all the others (mustard). Lake sediments that have associated relative paleointensity associated are shown as empty squares, and all others are shown as solid circles. (b) Temporal distribution of the geomagnetic field components derived from lake sediments for the past 4000 years; data are grouped in 100 year bins.

few marine) sediments from the CALS7K.2 data set has been expanded to include 18 additional studies, denoted by footnote c in Table 4. The previous directional record for Lake el Trebol [*Creer et al.*, 1983] has been replaced by a more recent study by *Irurzun et al.* [2006]. The entire data set now consists of 60 studies, and about one third of these also include relative paleointensity data (denoted by footnote b in Table 4). The resulting lake sediment data set (SED3k_dat0) contains over twice as many individual elements as the archeomagnetic one, and consists of 8316 (10739) declinations, 9030 (11563) inclinations, and 3029 (3943) intensities for the past 3000 (4000) years. The data distributions in space and time for SED3k are given in Figure 3. Once again there are more data in the vicinity of Europe

Table 3. Ten Data From GEOMAGIA50v2 Not Included in the Data Set[a]

UID	Site Name	Site Latitude	Site Longitude	Age	Declination	Inclination	Reference
1817	Checheno-Ingushetiia	43	44	−950	999	20.5	*Burlatskaya et al.* [1969]
2156	Nagomari	42.3	45.5	−750	345	20	*Burlatskaya and Chelidze* [1990]
3862	46-23-103: Feat. 247: Kaminaljuyu	14.7	269.5	250	275.6	27.2	*Eighmy and Sternberg* [1990]
3863	46-23-103: Feat. 261A: Kaminaljuyu	14.7	269.5	250	305.9	38.8	*Eighmy and Sternberg* [1990]
3864	CV30: Op. IX: Str. 191: Copan	14.8	270.8	300	0.9	32.7	*Eighmy and Sternberg* [1990]
3868	N rm. of Str. I-D: Tazumal	14	270.3	450	357.6	24.9	*Eighmy and Sternberg* [1990]
3869	46-23-103: Feat. 246B: Kaminaljuyu	14.7	269.5	450	278.2	22.1	*Eighmy and Sternberg* [1990]
3870	46-23-103: Feat. 246B: Kaminaljuyu	14.7	269.5	450	263.3	32	*Eighmy and Sternberg* [1990]
3871	46-23-103: Feat. 255: Kaminaljuyu	14.7	269.5	450	300.6	34.8	*Eighmy and Sternberg* [1990]
3872	PAC 78: Op. IV: Str. 71: Copan	14.8	270.8	450	357.3	24.6	*Eighmy and Sternberg* [1990]

[a] The unique identity (UID) is a number that links a datum with the corresponding entry in GEOMAGIA50v2.

than elsewhere, but the fraction of data in the Southern Hemisphere (almost 20%) is substantially larger than for ARCH3k. The temporal distribution is quite uniform except for a drop in numbers between 1600 A.D. and the present. This can be attributed to frequent loss or disturbance of material near the sediment/water interface during coring.

[17] Many recent sediment studies are dated by the radiocarbon method and have calibrated ^{14}C ages. In cases where uncalibrated ^{14}C ages were provided the program CALIB version 5 (http://calib.qub.ac.uk/calib/) [*Stuiver and Reimer*, 1993; *Reimer et al.*, 2004] was used for the calibration. Where applicable, the Southern Hemisphere and global marine calibration curves from CALIB5 were used. The two calibration programs Oxcal, used for some of the archeomagnetic data, and CALIB5 use the same calibration curves and we confirmed for a range of test ages that differences in calibrated ages resulting from the two programs are insignificant. All these lakes are denoted with the "C14" tag in the dating column of Table 4. A few older records were only available with calibrated ages from significantly older calibration curves [*Clark*, 1975], and a recalibration was not possible. These are denoted with the "C14oldcal" label. In a few cases varve counting was used as a dating tool ("varves" in Table 4), and in one case oxygen isotopes were also employed ("O18" in Table 4). The age scale of Lakes Trebol and Naroch had been geomagnetically tuned in the original publications. According to our policy of using only independently dated values we used the radiocarbon dates supplied with the record, which we calibrated and used to interpolate the age scale. Consequently for our application, Lakes Trebol and Naroch have age scales that differ by as much as a few decades from the final results presented by *Gogorza et al.* [2006], *Irurzun et al.* [2006], and *Nourgaliev et al.* [2005]. The declinations obtained from Lake Pepin [*Brachfeld and Banerjee*, 2000] are from individual core pieces that were not oriented, and so they have not been considered in this study.

[18] Another major change in the updated lake sediment data set is the consideration of relative paleointensity records and associated uncertainties that have been calibrated to an absolute scale following methods similar to *Korte and Constable* [2006a]. The calibration of relative intensities raises a number of questions, like whether a constant scaling factor over time is justified or whether the chosen reference model is suitable to give an unbiased scaling result. *Korte and Constable* [2006b] argue that a constant scaling factor seems justified by the fact that the resulting scatter in misfit to the calibrated intensity values is about the same as that for the absolute archeointensity data. Although non dipole field contributions cause a significant variability in intensity, on the millennial scale the dipole variation is clearly reflected in intensity time series. As our calibration factors are determined as medians over 3 ka we can expect reasonable results from a model reflecting the large-scale intensity variation. Note that constant calibration factors with time also mean that the influence of the model used for calibration on the relative intensity records is rather small, it acts just as an overall scaling but variations around that level on submillennial scales are purely determined by the sediment time series. It would seem preferable to include the determination of calibration factors as free parameters in the modeling, but because of the large data uncertainties and the comparatively small number of absolute intensity information this does not seem feasible at present.

[19] The scaling (LS scaling) adopted varied slightly depending on the model to be produced (see also the LS scaling column in Table 1). We devised our strategy to scale relative paleointensities, where possible, using intensity measurements from archeological artifacts, to avoid biases introduced by the models used for the scaling. In particular, data were scaled according to the ARCH3k model if the data sets included all the unconstrained lake sediment data (CALS3k and SED3k). This choice can be justified for Southern Hemisphere data if the average intensity is mainly determined by dipole strength rather than location (as seemed to be the case for the earlier CALS7K.2 model). In this case the absolute paleointensity for each lake sediment datum was determined using the ARCH3k model, then the ratio of the absolute paleointensity over the relative paleointensity was calculated. Finally, the median of the ratios was calculated and used as a scaling factor to convert the entire relative record into absolute paleointensity.

[20] In the case of the constrained CALS3k_cst data set, the scaling was based on the following scheme. First, all the absolute archeointensities in a 1000 km radius from the lake center were selected (see Figure 3a). If these were homogeneously distributed in time and overlapped with the same interval of the lake sediment data, then both lake sediments and archeological data were binned in 100 year intervals, the ratio of the archeointensities over the relative ones was determined for the entire time series, and the scaling factor determined as a

Table 4. Lake Sediment Records[a]

Abb.	Name	Region/Country	Reference	Latitude	Longitude	Age Range	N	Cst.	N_{REJ}	Dating
AD1[b,c]	Adriatic Sea	Italy	*Vigliotti* [2006]	42.6	14.5	10428 B.C. to 1606 A.D.	0/60/60	NAA	0/4/7	C14
AD2[b,c]	Adriatic Sea	Italy	*Vigliotti* [2006]	42.7	14.6	10609 B.C. to 1655 A.D.	0/39/41	NAA	0/14/12	C14
ANN	Lac d'Annecy	France	*Hogg* [1978]	45.8	6.2	350 B.C. to 1810 A.D.	167/167/0	NAA	51/10/0	C14oldcal
ARA	Lake Aral	Kazakhstan	*Nourgaliev et al.* [2003]	46.0	59.2	525 A.D. to 1675 A.D.	47/47/0	NAA	34/9/0	C14
ASL	Lake Aslikul	Russia	*Nourgaliev et al.* [1996]	54.4	54.1	2110 B.C. to 1445 A.D.	425/425/0	NAA	237/11/0	C14
BAI[b]	Lake Baikal	Siberia, Russia	*Peck et al.* [1996]	52.2	106.5	23679 B.C. to 1575 A.D.	24/24/24	NAA	16/2/7	C14
BAM	Lake Barombi Mbo	Cameroon	*Thouveny and Williamson* [1988]	4.5	9.5	23828 B.C. to 689 A.D.	49/49/0	MOD	28/38/0	C14
BAR[b]	Lake Barrine	N Queensland, AUS	*Constable and McElhinny* [1985]	−17.2	145.6	10331 B.C. to 925 A.D.	263/263/39	NLS	158/36/9	C14
BEG	Lake Begoritis	Greece	*Creer et al.* [1981]	40.8	21.8	3280 B.C. to 1950 A.D.	475/475/0	NAA	79/38/0	C14oldcal
BIR[b]	Birkat Ram	Israel	*Frank et al.* [2002b, 2003]	33.3	35.7	4403 B.C. to 1942 A.D.	157/157/151	NAA	84/69/59	C14+600 years
BIW	Lake Biwa	Japan	*Ali et al.* [1999]	35.3	136.0	7767 B.C. to 1683 A.D.	230/230/0	NAA	65/34/0	C14
BLM	Lake Bullenmerri	W Victoria, AUS	*Barton and McElhinny* [1981]	−38.2	143.1	9352 B.C. to 1742 A.D.	35/35/0	NLS	9/1/0	C14
BOU	Lac du Bourget	France	*Hogg* [1978]	45.7	5.9	250 A.D. to 1930 A.D.	146/146/0	NAA	33/0/0	C14oldcal
CAM	Brazo Campanario	Argentina	*Creer et al.* [1983]	−41.0	−71.5	5585 B.C. to 1361 A.D.	154/154/0	NLS	23/0/0	C14
DES	Dead Sea	Israel	*Frank et al.* [2007]	32.0	35.0	5021 B.C. to 1662 A.D.	301/301/0	NAA	172/137/0	C14
EAC[b]	Lake Eacham	N Queensland, AUS	*Constable and McElhinny* [1985]	−17.3	145.6	3747 B.C. to 1476 A.D.	536/536/247	NLS	365/129/130	C14
ESC[b,c]	Lake Escondido	Argentina	*Gogorza et al.* [2002, 2004]	−41.0	−71.3	15656 B.C. to 775 A.D.	50/50/38	NLS	22/3/15	C14
FAN	Lake Fangshan	China	*Zhu et al.* [1994]	40.2	116.0	16844 B.C. to 1454 A.D.	55/55/0	NAA	33/15/0	C14
FIS	Fish Lake	Oregon, USA	*Verosub et al.* [1986]	42.5	−118.9	9451 B.C. to 1803 A.D.	88/88/0	NAA	32/16/0	C14
FRG[b,c]	Frangsjön	Sweden	*Snowball et al.* [2007], *Snowball and Sandgren* [2002]	64.0	19.7	6670 B.C. to 1621 A.D.	95/95/107	NAA	53/1/70	varves
FUR[b,c]	Furskogstjärnet	Sweden	*Snowball et al.* [2007], *Zillén* [2003]	59.4	12.1	7462 B.C. to 1721 A.D.	105/105/100	NAA	53/3/83	varves+C14
GAR[b,c]	Gardar Drift	North Atlantic	*Channell et al.* [1997]	60.4	−23.6	6910 B.C. to 1955 A.D.	100/100/100	NLS	79/29/29	O18/C14
GEI	Llyn Geirionydd	Wales, UK	*Turner and Thomson* [1981]	53.0	−3.0	5150 B.C. to 1839 A.D.	99/99/0	NAA	24/2/0	C14
GHI[b,c]	Cape Ghir	NW Afr. Margin	*Bleil and Dillon* [2008]	30.9	−10.3	5411 B.C. to 1811 A.D.	101/101/101	NAA	42/33/67	C14
GNO	Lake Gnotuk	W Victoria, AUS	*Barton and McElhinny* [1981]	−38.2	142.9	9421 B.C. to 831 A.D.	84/84/0	NLS	22/9/0	C14
GRE[c]	Greenland	North Atlantic	*Stoner et al.* [2007]	67.1	−30.8	9772 B.C. to 748 A.D.	282/282/0	NAA	253/96/0	C14
HUR	Lake Huron	Great Lakes, USA	*Mothersill* [1981]	44.0	−82.0	14021 B.C. to 1460 A.D.	265/265/0	NAA	213/41/0	C14
ICE[c]	Iceland	North Atlantic	*Stoner et al.* [2007]	66.6	−20.9	9583 B.C. to 1560 A.D.	688/688/0	NAA	399/179/0	C14
KEI	Lake Keilambete	W Victoria, AUS	*Barton and McElhinny* [1981]	−38.2	142.9	10327 B.C. to 1912 A.D.	304/304/0	NLS	93/35/0	C14
LAM	Lake Lama	Siberia, Russia	*Frank et al.* [2002a]	69.5	90.2	17334 B.C. to 1664 A.D.	171/184/0	MOD	146/20/0	C14
LEB[b]	Lake LeBoeuf	USA	*King* [1983]	41.0	−80.0	2773 B.C. to 1830 A.D.	36/36/344	NAA	15/2/138	C14
LOM	Loch Lomond	Scotland, UK	*Turner and Thomson* [1979]	56.0	−5.0	4885 B.C. to 1838 A.D.	99/99/0	NAA	29/0/0	C14

Table 4. (continued)

Abb.	Name	Region/Country	Reference	Latitude	Longitude	Age Range	N	Cst.	N_{REJ}	Dating
LSC[b]	Lake St. Croix	Minnesota, USA	*Lund and Banerjee* [1985]	45.0	−93.0	8674 B.C. to 1859 A.D.	197/197/222	NLS	134/11/78	C14
MAR	Mara Lake	British Columbia, CAN	*Turner* [1987]	50.8	−119.0	3529 B.C. to 1861 A.D.	177/177/0	NAA	97/47/0	C14
MEE	Meerfelder Maar	Germany	*Brown* [1981]	49.0	7.0	15050 B.C. to 1843 A.D.	181/181/0	NAA	79/66/0	varves
MEZ[b,c]	Lago di Mezzano	Italy	U. Frank (personal communication, 2007)	42.6	11.9	4105 B.C. to 1774 A.D.	207/221/212	NAA	73/26/43	C14
MNT	Lago Morenito	Argentina	*Creer et al.* [1983]	−41.0	−71.5	10331 B.C. to 1424 A.D.	158/158/0	NLS	29/15/0	C14
MOR	Lac Morat	Switzerland	*Hogg* [1978]	46.9	7.1	110 B.C. to 1590 A.D.	153/153/0	NAA	52/5/0	C14oldcal
MOT[b,c]	Mötterudstjärnet	Sweden	*Snowball et al.* [2007], *Zillén* [2003]	59.7	12.7	7764 B.C. to 1811 A.D.	104/104/104	NAA	64/3/81	varves+C14
NAR[b]	Lakes Naroch+Svir	Belorussia	*Nourgaliev et al.* [2005]	54.8	26.6	9970 B.C. to 902 A.D.	133/133/0	NAA	41/8/0	C14
NAU[b,c]	Nautajärvi	Finland	*Snowball et al.* [2007], *Ojala and Saarinen* [2002]	61.8	24.7	7900 B.C. to 1980 A.D.	93/93/93	NAA	34/6/8	varves
PAD[b]	Palmer Deep	Antarctic Peninsula	*Brachfeld et al.* [2000]	−64.9	−64.2	7333 B.C. to 1755 A.D.	691/691/631	NAA	682/507/142	C14
PEP[b,c]	Lake Pepin	USA	*Brachfeld and Banerjee* [2000]	44.4	−92.1	6196 B.C. to 1964 A.D.	0/591/610	NLS	0/13/228	C14
POH[b]	Pohjajärvi	Finland	*Saarinen* [1998]	62.8	28.0	1291 B.C. to 1950 A.D.	109/109/109	NAA	59/16/31	varves
POU	Lake Pounui	N Island, New Zealand	*Turner and Lillis* [1994]	−41.1	175.0	600 B.C. to 1759 A.D.	47/47/0	MOD	19/16/0	C14
SAR[b,c]	Sarsjön	Sweden	*Snowball et al.* [2007], *Snowball and Sandgren* [2002]	64.0	19.6	7000 B.C. to 1600 A.D.	92/92/92	NAA	66/5/61	varves
SAV[b]	Savijärvi	Finland	*Snowball et al.* [2007], *Ojala and Tiljander* [2003]	61.8	24.7	8250 B.C. to 1000 A.D.	41/41/0	NAA	22/3/0	varves
STL[b,c]	St. Lawrence Est.	CAN	*St-Onge et al.* [2003]	48.6	−68.6	6555 B.C. to 1197 A.D.	459/442/459	MOD	354/36/39	C14
SUP	Lake Superior	Great Lakes, USA	*Mothersill* [1979]	48.5	−89.0	11908 B.C. to 1850 A.D.	179/179/0	NLS	119/45/0	C14
TRE[b,c]	Laguna el Trebol	Argentina	*Irurzun et al.* [2006], *Gogorza et al.* [2006]	−41.1	−71.5	35457 B.C. to 1639 A.D.	78/78/59	NLS	14/4/40	C14
TRI	Lake Trikhonis	Greece	*Creer et al.* [1981]	38.6	21.5	4687 B.C. to 1899 A.D.	718/718/0	NAA	146/57/0	C14oldcal
TUR	Lake Turkana	Kenia	*Barton and Torgersen* [1988]	2.6	36.6	743 B.C. to 1969 A.D.	0/100/0	NLS	0/34/0	C14
TY1[c]	Tyrrhenian Sea	Italy	*Vigliotti* [2006]	42.6	9.9	3015 B.C. to 1886 A.D.	48/48/0	NAA	22/13/0	C14
TY2[c]	Tyrrhenian Sea	Italy	*Vigliotti* [2006]	42.9	9.9	3604 B.C. to 1874 A.D.	47/49/0	NAA	7/8/0	C14
VAT	Vatndalsvatn	Iceland	*Thomson and Turner* [1985]	66.0	−23.0	4837 B.C. to 1377 A.D.	100/100/0	NLS	73/11/0	C14
VIC	Lake Victoria	Uganda	*Mothersill* [1996]	0.0	32.4	5637 B.C. to 1850 A.D.	112/116/0	NLS	49/27/0	C14
VOL	Lake Volvi	Greece	*Creer et al.* [1981]	40.8	23.5	539 B.C. to 1877 A.D.	821/821/0	NAA	260/69/0	C14oldcal
VUK	Vuokonjärvi	Finland	*Huttunen and Stober* [1980]	63.4	29.1	4995 B.C. to 1763 A.D.	37/55/0	NAA	22/7/0	varves
WAI	Lake Waiau	Hawaii, USA	*Peng and King* [1992]	19.8	−155.5	13111 B.C. to 1836 A.D.	61/61/0	NAA	6/10/0	C14
WIN	Lake Windermere	N England, UK	*Turner and Thomson* [1981]	54.3	−3.0	9596 B.C. to 611 A.D.	65/65/0	NAA	27/1/0	C14

[a] The abbreviation (Abb.) represents the filename used. The lake name, the country and geographical position are given. The age range indicates the time interval covered by the core. For our model, the cores were truncated at 2000 B.C. The number of data are given in N as declination/inclination/intensity, and the dating technique used is shown in the dating column. The amount of rejected data N_{REJ} is also given in terms of declination/inclination/intensy, and the constrain column (Cst.) shows the criterion for the rejection (see also text), where NAA means neighbor archeological artifacts, NLS means neighbor lakes, and MOD means ARCH3k.1 model. Notice that in cases where no data were available for a particular bin, then the model was used as a criterion.

[b] Accompanying relative intensity record.

[c] Record was not in CALS7k.2.

median of the ratios. If no archeological artifacts were available, then the ARCH3k model was used in a similar way as for the unconstrained cases. The choice of the 100 year bin width is motivated by the fact that the scaling of the relative paleointensities needs to follow the long-term trend of the curve, and not its fine structure.

[21] Figure 3a indicates the distribution of lake sediments around the globe. Lakes that have enough archeological artifacts for calibration within a 1000 km radius are denoted in blue, and are located, as expected, at midlatitudes in the Northern Hemisphere. All other lakes are denoted in mustard, and clearly show their importance in filling serious gaps in the whole Southern Hemisphere and at higher northern latitudes. The lakes that have associated intensity measurements are shown as squares, and appear to be randomly distributed around the globe. Figure 3b shows the temporal distribution of the three geomagnetic field components derived from lake sediments. We notice that the lake sediments are distributed more homogeneously in time than the archeological artifacts.

3. Accuracy and Uncertainty Assignments

[22] In this section we discuss the assignment of uncertainties to the observations that make up the ARCH3k and SED3k data compilations. Although many data are published with their own uncertainty estimates, others are not, and it is important for any regional or global modeling purposes that the uncertainty estimates of the data sets are internally consistent. This allows data used for modeling to be weighted in a consistent way according to their uncertainties.

[23] Uncertainties for paleomagnetic data are usually given in terms of standard deviation of the intensity, of the age, and as the α_{95} confidence circle of the direction. As previously discussed by *Korte et al.* [2005], gathering information from existing publications can reveal problems associated with the uncertainties of the data. In many cases the information is missing; and where it is available a wide array of analyses is possible. Some authors, for example, use the number of samples to calculate the associated α_{95}, others prefer to use the number of specimens, and because the α_{95} is inversely related to number of measurements, the latter strategy would result in an underestimation of the confidence circle. For the modeling procedure, all the α_{95} were converted to standard deviations of the declination and inclination (σ_D and σ_I) using the following formulae after *Piper* [1989]:

$$\sigma_I = \frac{81}{140}\alpha_{95} \tag{1}$$

and

$$\sigma_D = \frac{81}{140 \times \cos I}\alpha_{95} \tag{2}$$

[24] For paleointensity the average and its standard deviation are calculated according to the number of specimens. In several studies, however, the standard error (s) has been given, and so, when the individual results were tabulated, a standard deviation σ was recalculated using the formula:

$$\sigma = s \times \sqrt{n} \tag{3}$$

n being the number of specimens used in the calculation of the mean.

[25] *Valet* [2003], *Korte et al.* [2005], *Donadini et al.* [2007], and more recently *Genevey et al.* [2008] discuss in detail the problems related to paleointensity determinations. In general these are related to subjective interpretations of the Arai diagrams [*Arai*, 1963] which often lead to overestimations of the paleointensities when only the lower temperature steps are taken into account; or to the arbitrary use of the cooling rate and anisotropy corrections. In some cases, for example for the Bulgarian data set, many uncertainties have been revised after inclusion of new measurements or after the recalibration of the ^{14}C age, and so in these cases the new uncertainties differ from the originally published ones. Only the new, revised uncertainties were used. Lake sediments certainly provide a significant contribution to the total data set. However, their uncertainties can in general be expected to be larger than those of archeological artifacts, because the sampling methods do not allow for maximum orientation precision. Declination is hard to constrain, and the risk that a piston corer does not reach the lake bottom exactly vertical is high, which can bias the inclination when relying on data from individual cores. Relative paleointensity determinations could be determined more rapidly compared to the classical paleointensity methods, but have always been treated with some suspicion because of uncertainties related to the acquisition of magnetization in sedimentary environments [*Tauxe*, 1993]. In a recent study, *Tauxe et al.* [2006] point out that the remanent magnetization of sediments might not always be as linearly related to the geomagnetic field strength as

is hoped. On the other hand, if sedimentary records can be validated by other records from nearby locations, or by other paleomagnetic data [e.g., *Snowball et al.*, 2007; *Ojala and Saarinen*, 2002; *Donadini and Pesonen*, 2007] a good approach to reduce biases would consist of comparing several independent records and assessing their consistency.

[26] Similar considerations to those cited above led *Korte et al.* [2005] to assign minimum uncertainties to the data to avoid discrimination introduced by incompatible calculations of the uncertainties. Overly optimistic uncertainty estimates are a particular concern in models using the technique of minimizing a quadratic measure of misfit based on least squares. *Korte et al.* [2005] determined separate minimum directional uncertainties for archeological and sediment data by studying RMS deviations of D and I from the gufm1 model in the 1590–1990 A.D. time interval. We follow a similar but not identical strategy. For modeling purposes all data that have no associated error were assigned a minimum α_{95} of 4.3° for archeomagnetic directions and 6° for lake sediments, or a σ_{Ba} of 5 μT. Any data with α_{95} smaller than 4.3° (or 6°), or σ_{Ba} smaller than 5 μT were also assigned these minimum uncertainties. The conversion of α_{95} to σ_I and σ_D (via equations (1) and (2)) means that even the minimum declination uncertainty varies with location depending on the local inclination. The minimum value of 1.5 μT assigned by *Korte et al.* [2005] for intensity data also seemed too optimistic, and so we adopt our new value of 5 μT.

[27] The distribution of uncertainties assigned to directions, intensities, and ages, are presented in Figure 4, both for the archeological artifacts (Figures 4a–4c) and the lake sediments (Figures 4d–4f) of the past 3000 years. The pie charts for directions and intensities accuracies distinguish 3 groups. Data that have no uncertainty associated are marked in blue and labeled as "Not Spec."; data whose uncertainties are lower than the threshold values (4.3 and 6°, 5 μT) are marked in green, whereas data with large uncertainties are left unchanged and are marked in red. Additionally, Figures 4c and 4f show the age uncertainties gathered in five groups as shown by *Korte et al.* [2005]. Unlike *Korte and Constable* [2005] our models initially take no account of the age uncertainties, however, we do use age uncertainty as a constraint in data selection as well as in estimating model uncertainties, so we report this information here.

[28] We notice a substantial difference between archeological artifacts and sediments. Archeological artifacts mainly show values that are lower than the threshold minima, indicating that perhaps the assigned values are too optimistic, and so only 10 to 15% of the data uncertainties are kept as in the original publication. On the other hand, lake sediments show a larger variation. Most direction uncertainties were not specified for lake sediments and so were set to 6°, whereas only 11% of the intensity data has larger uncertainties than the 5μT. The accuracies of the intensity values presented for the lake sediments (Figure 4e) are calibrated along with the data, following the method described in the previous section and it appears that about 70% of the data has uncertainties lower than 5μT. Because the modeling strategy weights data according to the uncertainties, it is important to note that most of the data are assigned uncertainties that result in equal weights for the data within each group. Age uncertainties appear to be dominated by the 10–50 year group. The vast majority of data have age uncertainties lower than 100 years (99% of the data set). Age uncertainties also depend on the provenance of the finds: artifacts from regions with well constrained archeological/historical backgrounds (e.g., Europe, Asia) have better dating. For the ARCH3k data GEOMAGIA50v2 allows querying for additional metadata such as material, paleointensity technique, dating methods, number of samples/specimen measured. These metadata could also be used to create constrained data sets. However, we decided not to use these additional criteria in our constraining strategy because (1) SED12k has no information about these metadata (yet) and (2) it was not possible to recover these metadata for some of the published studies included in GEOMAGIA50v2.

4. Selected Data Sets for Modeling

[29] In this study we created a series of data sets as outlined in Table 1 by including/excluding a particular recorder (archeological artifacts or lake sediments), or by constraining the data set to reject data with large uncertainties. Subsequently, each data set was further modified by a statistically based rejection of outliers to an initial model. The five initial data sets are denoted as version 0. After producing a preliminary version 0 model, an analysis of residuals was carried out, and outliers were rejected on the basis of the 3-sigma rule [*Cramer*, 1999], i.e., for normally distributed residuals rejecting data that would lie outside the 99% confidence interval. After the statistical rejection of outliers, a new series of models (version 1) was produced.

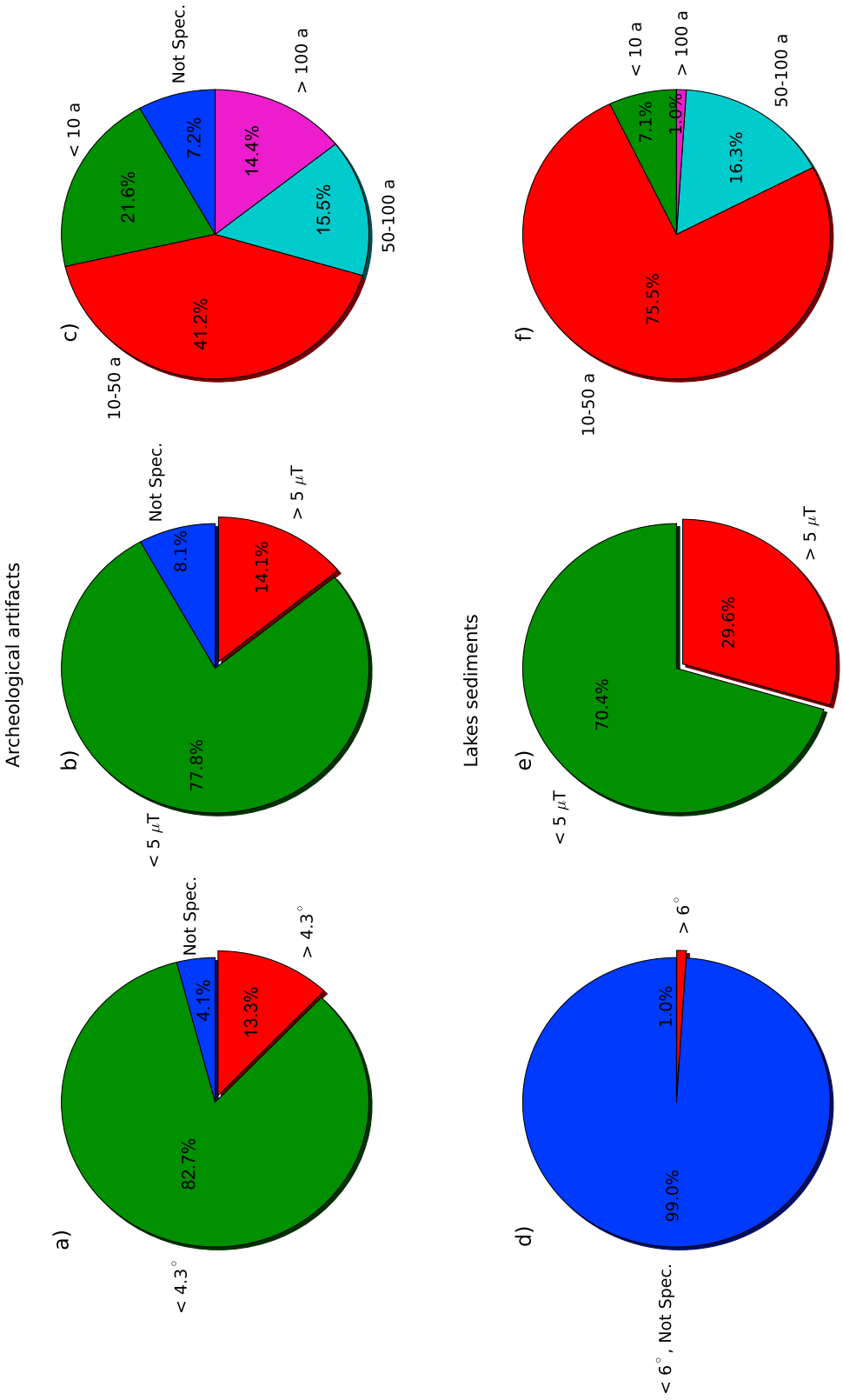
Archeological artifacts
Lakes sediments
a)
< 4.3°
Not Spec.
4.1%
82.7%
13.3%
> 4.3°
b)
< 5 μT
Not Spec.
8.1%
77.8%
14.1%
> 5 μT
c)
10-50 a
< 10 a
Not Spec.
21.6%
7.2%
41.2%
14.4%
15.5%
> 100 a
50-100 a
d)
< 6°, Not Spec.
99.0%
1.0%
> 6°
e)
< 5 μT
70.4%
29.6%
> 5 μT
f)
10-50 a
< 10 a
> 100 a
7.1%
1.0%
75.5%
16.3%
50-100 a

Figure 4

Table 5. Number of Data Available in Each Selection for Both the Past 3000 and the Past 4000 Years

	3000 Years				4000 Years			
Data Set Name	Declination	Inclination	Intensity	Total	Declination	Inclination	Intensity	Total
ARCH3k_dat0	2761	4174	2670	9605	2877	4304	3001	10182
ARCH3k_dat1	2715	4129	2639	9483	2827	4253	2964	10044
ARCH3kcst_dat0	1942	2969	1300	6211	1991	3022	1423	6436
ARCH3kcst_dat1	1911	2929	1282	6122	1960	2981	1401	6342
SED3k_dat0	8316	9030	3029	20375	10739	11563	3943	26245
SED3k_dat1	8174	8919	2997	20090	10521	11438	3893	25852
CALS3k.3_dat0	11077	13204	5699	29980	13616	15867	6944	36427
CALS3k.3_dat1	10892	13055	5638	29585	13321	15703	6859	35883
CALS3kcst_dat0	6149	10415	3344	19908	7320	12500	3989	23809
CALS3kcst_dat1	6039	10335	3313	19687	7194	12413	3949	23556

4.1. Version 0 Data Sets

[30] The main difference among the data sets is the use of either lake sediments or archeological artifacts, or both. These two groups are very different: the archeological artifacts represent a point in time and can be quite spatially dispersed, whereas the lake sediments yield time series of geomagnetic field parameters from individual locations. The global distribution of the two groups is also very different: whilst the archeological artifacts are clustered in Europe and Asia, with a few exceptions in N America, Peru, Hawaii, and Australia, the lake sediments are spread more homogeneously around the globe. Therefore we expect to find significant differences among the models.

4.1.1. All Archeological Artifacts Data Set: ARCH3k_dat0

[31] This data set consists of all available archeomagnetic data covering the past 3000 years included in the GEOMAGIA50v2 database. The features of this data set have already been discussed in section 2.1. The statistics concerning each data set are reported in Table 5.

4.1.2. Constrained Archeological Artifacts Data Set: ARCH3kcst_dat0

[32] To investigate the effect of data selection/rejection on the data sets, a set of simple reliability criteria was applied to the ARCH3k_dat data set using the uncertainties recalculated in the database. In this case, only data with $\alpha_{95} \leq 10^{\circ}$, $\sigma_{VADM} \leq 2 \times 10^{22}\mathrm{Am}^2$ and a $\sigma_{AGE} \leq 100$ years were kept. It turns out that 3394 data are rejected from the original data set (Tables 5 and 6).

4.1.3. Lake Sediments Data Set: SED3k_dat0

[33] This data set consists of all lake sediment data, as described in section 2.2. The data set consists of 8316 declinations, 9030 inclinations, and 3029 intensities calibrated using the ARCH3k model (see Tables 1 and 5).

4.1.4. All Archeological Artifacts and All Lake Sediments: CALS3k.3_dat0

[34] This data set is a combination of the ARCH3k_dat0 (all archeological data) and the SED3k_dat0 (all lake sediment data). Models for the same age range, but with different data sets, have already been produced and described by *Korte and Constable* [2003, 2005], and are available up to version 2. We expect that our CALS3k.3.0 model should be comparable in large scale to the CALS3k.2 version [*Korte and Constable*, 2005], but with substantially improved resolution as measured by the model spherical harmonic spectra [*Korte et al.*, 2009, Figure 8]. The new CALS3k.3 data set includes

Figure 4. Pie charts presenting the fractions of data belonging to a particular group of uncertainty. Groups are defined according to the threshold values set for the modeling, i.e., 4.3° for the α_{95} of directions from archeological artifacts, 6° for the α_{95} of directions from lake sediments, and 5 μT for the intensities (both archeological artifacts and lake sediments). Data that have smaller uncertainties than the threshold values are shown in green, whereas the ones that have larger uncertainties are shown in red. Values that have no uncertainty associated are also presented in blue. In addition, the uncertainty of dates is divided into the groups proposed by *Korte et al.* [2005] (see text for details). (a) Directional uncertainties of archeological artifacts, (b) intensity uncertainties of the archeological artifacts, and (c) archeological dating uncertainties. (d) Directional uncertainties of lake sediments. Notice that two uncertainty groups (Not Spec. and ≤6°) are merged. (e) Intensity uncertainties of the lake sediments and (f) sediment dating uncertainties.

Table 6. Percentage of Data Covering the Past 3000 Years, Rejected on the Basis of the Residual Analysis or on the Selection Criteria[a]

	Basis of % Rejected Data	
Starting Data Set	Outliers (Version 1)	Data Selection (Constrained Version)
ARCH3k_dat0 (N = 9605)	ARCH3k_dat1 (N = 9483), 1.3%	ARCH3kcst_dat0 (N = 6211), 35%
SED3k_dat0 (N = 20375)	SED3k_dat1 (N = 20090), 1.4%	SED3k_cst.0 (N = 13697), 33%
CALS3k.3_dat0 (N = 29980)	CALS3k_dat1 (N = 29585), 1.3%	CALS3kcst_dat0 (N = 19908), 34%

[a] Constrained data selection removes a larger amount of data than the statistical rejection of outliers. The amount of data N for each data set is also indicated.

10604 (9023 lake sediments and 1581 archeological artifacts) new data (3481 declination, 3740 inclination, and 3383 intensity) for the past 3000 years.

4.1.5. Constrained Archeological Artifacts and Lake Sediments: CALS3kcst_dat0

[35] This data set groups the constrained ARCH3kcst_dat0 archeological data set and a constrained data set of lake sediments (SED3k_cst.0), and has the most complex set of constraints. As we pointed out in section 3, the uncertainties of the lake sediments are in general larger than those for archeological artifacts. In several cases we also observe inconsistencies either within the record, or when compared with either archeological artifacts or with other lake sediments in the neighborhood. To overcome this problem, lake sediment values were checked against other available data in a 1000 km radius from the lake location, or alternatively against the ARCH3k.1 model (all archeological data). Note that the difference between intensity calibration by ARCH3k.1 or ARCH3k cst.1 is insignificant. Because of the inhomogeneity of the spatial distribution of the observations, we distinguish the following three cases for the comparison.

[36] In the first case the lake is located in a region that is rich in archeological measurements. Both lake sediment data and the archeological artifacts were binned in 50 year intervals. In order to eliminate the latitudinal difference caused by the axial dipole field contribution for this comparison, we transformed intensity values to virtual axial dipole moments (VADMs) and inclinations to inclination anomalies (ΔI). The ΔI is calculated as the difference between the observed (I_{Obs}) and geocentric axial dipole (I_{Ax}) inclination:

$$\Delta I = I_{Obs} - I_{Ax} \quad (4)$$

where:

$$I_{Ax} = \tan^{-1}(2\tan(\lambda)) \quad (5)$$

λ being the site latitude. Then, each lake sediment datum was compared with the average declination, inclination, or VADM of the corresponding binned archeological data. However, if a particular bin did not contain enough data ($\leq$3), then the ARCH3k model was used for the comparison. In the second case, the lake lies in a location where not enough archeological data are available (mustard lakes on Figure 3a); however, it is possible to check the data consistency with other nearby lakes. This was possible for the following lakes: ESC, TRE, CAM, MNT (Argentina); LSC, PEP, SUP (North America), GNO, BLM, KEI (South Australia), BAR, EAC (North Australia), VAT, GAR (Iceland), VIC, TUR (Africa). Again, the data from the neighboring lakes are binned in 50 year intervals, and then the declinations, inclination anomalies, and intensities are compared. In cases where data were not overlapping in time a comparison with the ARCH3k.1 model was performed. In the third case the lake is located in an isolated site, and so the data are compared with the ARCH3k.1 model only. We realize that this latter comparison might not be based on a completely sound assumption, because it implies that the ARCH3k.1 model is valid at sites where there is no coverage by archeological data. We motivate this choice by the fact that the general long-term structure of all models are similar, as we will show in the examples later.

[37] For each of the three cases, data were discarded if the differences exceeded 10° for directions, 2×10^{22}Am^2 for intensities, or 100 years for the dating. Notice that the rejections affected a single component, and not the full vector; for example, if one data consists of a declination that differs from the model by more than 10°, and a inclination that differs less than 10°, then only the declination was rejected. These selection criteria, although "loose," reject 34% of the data (10072 data rejected from CALS3k_cst0 data set for the past 3000 years). Table 4 shows the constraining criterion (neighboring archeological artifacts, neighboring lakes, or

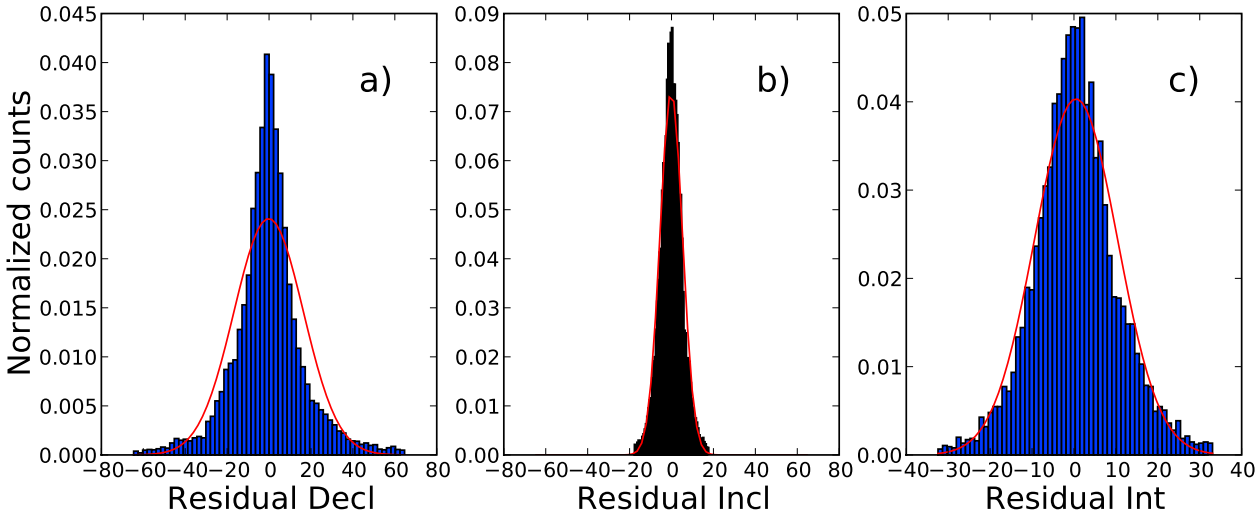

Figure 5. Histograms showing the normalized distribution of residuals arising from the difference CALS3k.3 model predictions and CALS3k.3_dat1 observations. (a) Declinations, (b) inclinations, and (c) intensities. All data are binned in 50 year intervals. Blue bars represent observations per bin, whereas the red line is the normalized probability density function calculated using the mean and standard deviation obtained for each component.

ARCH3.1 model) for each lake, and the number of rejected data for each component.

4.2. Statistical Rejection of Outliers: Version 1 Data Sets

[38] The version 0 data sets were used to produce the same number of version 0 models (Table 1). The quality of the fit of the model is measured by the root mean square misfit [*Korte et al.*, 2009, section 4]. Ideally, the constrained data selection scheme presented here would remove any discordant data that produce outliers from the model. This was tested by performing an analysis of the residuals and then creating new data sets that were used for the outlier-free version 1 models. Statistical rejection of outliers was performed in the following way. We calculated the corresponding model prediction for each datum over the entire 4000 year period, and created a residuals file that included the differences between observations and corresponding predictions. We calculated the mean and the standard deviation of the residuals of each data set, and all data lying outside of three times the standard deviation (i.e., the 99% confidence interval assuming a Gaussian distribution) were rejected. Figure 5 shows the distribution of the residuals for each component after outlier rejection. The red line presents the normalized probability density function calculated using the derived mean and standard deviation of the residuals. In all cases the residuals are symmetric around the mean, but can show a variable amount of kurtosis.

[39] Table 7 shows the statistics of the residual analysis for each data set for the time interval 0–4 ka. We notice that in general this statistical selection lowers the RMS misfit and helps center the mean of the residual distribution around 0, as expected. In the following, we also show that the residual analysis reveals very few outliers: about 1.5% of the data from each version 0 are removed as outliers. The percentage of outliers in all models is quite similar regardless of whether the initial data set is constrained or not. However, Table 7 shows that outlier rejection can have a larger impact on the RMS residual for the unconstrained data sets.

[40] The geographic distribution of data is shown in Figure 6 for the various data sets as a contoured map of concentration of observations. Figure 6 (left) represents the density of data (log scale) for the final data sets (version 1) after rejection of outliers, whereas Figure 6 (middle) shows the distribution of the data rejected using the constraints applied to ARCH3kcst_dat0, CALS3kcst_dat0 and SED3kcst_dat0; and Figure 6 (right) gives distributions for the outliers. There is no strong geographic bias in the data rejected by either the uncertainty measures or the residual analysis for outliers. Table 8 gives the number of data rejected by the statistical analysis of outliers.

5. Data Sets and Model Fits

5.1. Regional Fits to the Data

[41] In this section we discuss how the models fit the data in various regions. First, we compare the

Table 7. Residual Analysis of the Original Data Sets Covering the Past 4000 Years Expressed in Terms of Mean and Standard Deviation σ of the Three Components

	Declination		Inclination		Intensity	
Data Set Name	Mean	σ	Mean	σ	Mean	σ
ARCH3k_dat0	−0.22	7.62	−0.13	4.76	0.71	9.66
ARCH3kcst_dat0	0.04	6.28	−0.11	4.22	0.20	8.13
SED3k_dat0	1.20	23.44	−0.14	6.05	0.67	11.11
CALS3k.3_dat0	0.50	21.56	−0.16	5.94	0.83	11.02
CALS3kcst_dat0	0.59	8.70	−0.14	4.63	0.41	7.41
ARCH3k_dat1	−0.15	6.11	0.03	4.17	0.35	8.63
ARCH3kcst_dat1	0.01	5.27	−0.01	3.61	0.01	7.18
SED3k_dat1	0.47	18.59	−0.14	5.50	0.41	9.89
CALS3k.3_dat1	−0.18	16.56	−0.13	5.39	0.50	9.89
CALS3kcst_dat1	0.24	7.45	−0.14	4.37	0.25	6.89

models at a series of different lake locations, because these are more homogeneously distributed, and also because we can show easily how the data selection worked in a range of different situations. Because of their more homogeneous spatial and temporal distribution, sedimentary data influence all of the SED3k, CALS3k, and CALS3k_cst models. Figures 7–9 show three illustrative cases of the analysis, corresponding to excellent overall data coverage, a region dominated by several lake records, and an isolated lake record. Additionally, Figure 10 shows a case where no lake data are available, and Figure 11a shows case with discrepant data. For comparison, the CALS7K.2 model of *Korte and Constable* [2005] is always shown. In every case, the new models contain more structure than CALS7K.2 of *Korte and Constable* [2005].

[42] The first case (Figure 7) presents the outcome of the 10 different models at Mezzano lake, in Italy. The archeological artifact observations within a 1000 km radius around the lake center (red and black circles) show good agreement with the selected lake sediments (solid green circles); lake sediments data that are rejected on the basis of constrained data selection are shown as open green circles. In this case, only a few lake sediment data were rejected for the constrained model CALS3k_cst. The models are presented as 5 pairs of different color. The version 0 models are presented as dashed lines, and version 1 as solid. For comparison, Figure 7 also shows the mixed VADM/VDMs for the western European region derived by *Genevey et al.* [2008]. We notice that in general there is good agreement between the model and the weighted VADMs, with the exception of the period 1600–1800 A.D. and one point at 900 A.D. Several other features of Figure 7 are noteworthy. Firstly, the outlier rejection has little visible effect on the models. Differences between SED3k and the ARCH3k models are greatest in the declination record for 1000–500 B.C. and 900–1700 A.D. time intervals, where the main differences between the archeological artifacts and the lake sediment data are also visible. As might be expected there is a tendency for the CALS3k models to lie between the ARCH3k and SED3k models in response to competing data fitting requirements. In general the SED3k model (blue) does not do a particularly good job of fitting these lake sediment data (green). The largest deviations occur in time periods (e.g., 500–1000 A.D.) where nearby lakes are inconsistent with Mezzano data.

[43] The second case (Figure 8) shows the outcome of the models in Argentina. The four lakes Escondido (ESC), Trebol (TRE), Brazo Campanario (CAM), and Morenito (MNT) are located very close to each other. In this case the selection of data for CALS3k_cst was performed by comparing the values from the different lakes. This strategy is quite efficient at getting rid of inconsistent data (open circles), especially the undesirable end effects at the youngest part of the core. The five pairs of models are also shown for the location of lake Escondido. In this case the outlier rejection leads to some differences between version 0 and version 1 models, especially for ARCH3k_cst in inclination at around 300–600 A.D. and among all archeomagnetic models in the declination and VADMs. For the period 1000 B.C. to 0 A.D. there is poor agreement in declination between predictions of the archeomagnetic model and both the other models and sediment data.

[44] The third case (Figure 9) represents the case of Lake Pounui in New Zealand. This lake is isolated, meaning that there are too few archeological artifact

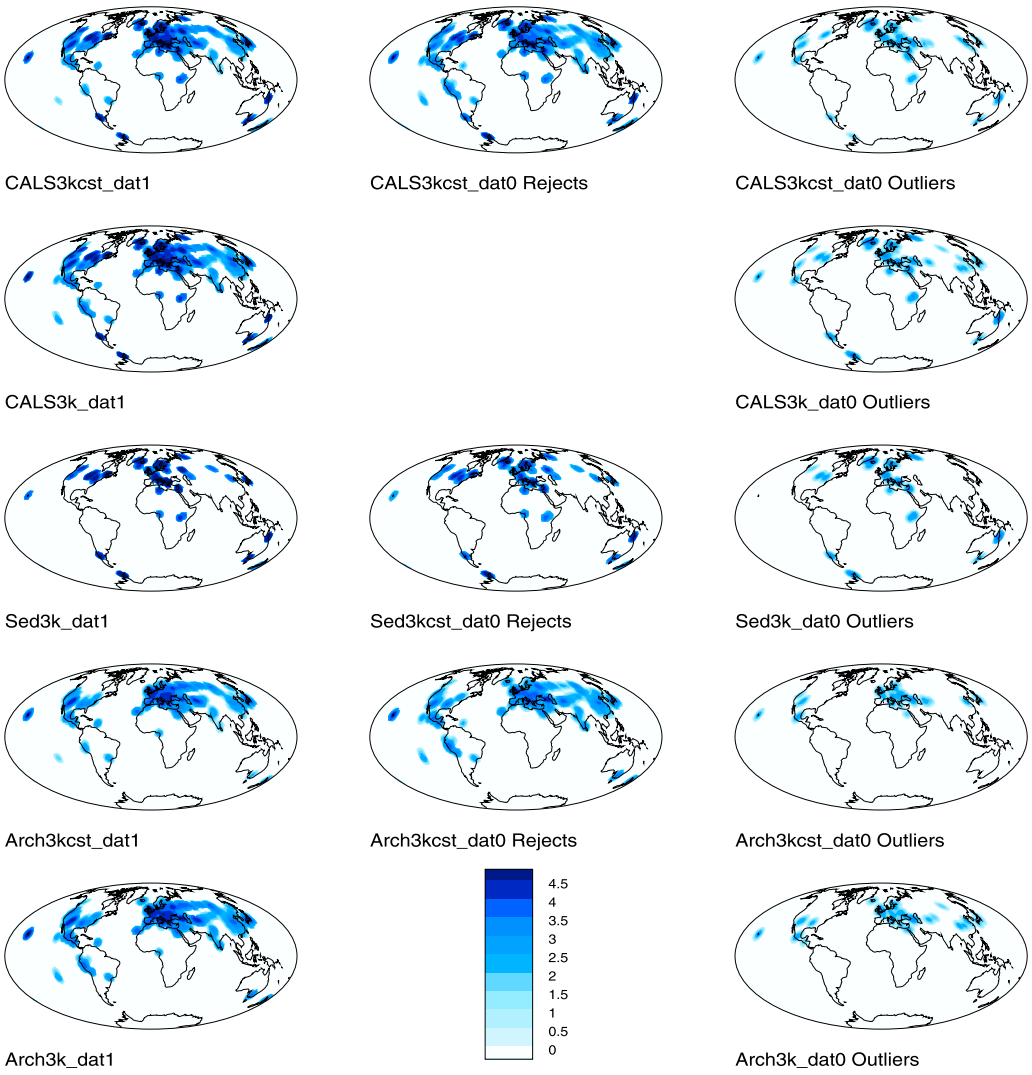

Figure 6. Global data distributions for the five data sets used to create the final spherical harmonic models. The distributions are constructed by contouring the logarithm of data concentration by area, in effect a kind of density function for observations (see *Korte et al.* [2005, section 4] for details). The logarithmic scale is such that the integral over the whole sphere returns the total number of data points for the past 4000 years given in Tables 5 and 7. (left) The final data sets after rejection of outliers and (right) distributions for the outliers. (middle) The distributions of the data that are rejected on the basis of the constraints described in the text.

data nearby and no other lake sediments that can be used for meaningful regional comparisons. No intensities are available for this lake. This case shows that the differences among models are more significant in regions with low number of measurements. As in the Argentine case, the constrained archeological model has large declination swings; here around 300–600 A.D. It also shows a negative inclination anomaly at 200 B.C. when all other models predict a positive one. The other constrained model (CALS3k_cst.1) appears to follow the inclination outcome of the archeological model ARCH3K.1, suggesting that the rejection of lake sediment data in that region leads to a more significant influence of the archeological artifacts. This might indicate that the rejection of data can bias model outcomes significantly in regions that are already poor in data, and in this sense removing data with large uncertainties might not be the best strategy for producing global models.

[45] In the eastern Asia region (Figure 10) we notice that the two archeological models fit the low declinations around 800–1200 A.D. well, whereas the sediments predict a rather smooth curve. The two models derived from both the lake sediments and the

Table 8. Number of Data Rejected on the Basis of the Statistical Analysis of Outliers for the Time Period Between −2000 and 1990

Data Set Name	Declination	Inclination	Intensity
ARCH3k_dat1	50	51	37
ARCH3kcst_dat1	31	41	22
SED3k_dat1	218	125	50
CALS3k.3_dat1	295	164	85
CALS3kcst_dat1	126	87	40

archeological artifacts have a behavior intermediate between the other models. Also in this case the mixed VADMs fit the ARCH3k and ARCH3k_cst models rather well.

[46] The Hawaiian region is also worth mentioning, as it demonstrates the discrepancies between the lava flows (from Kilauea volcano) and the lake sediments (from lake Waiau; Figure 11). Waiau has no intensity data. The sediment model generally predicts lower intensities than the other models. In this region the VADM also appear to be higher on average than any model predictions. Declinations show the most similar features among models, with the exception of the period around 500 B.C., where the lavas show a minimum not reflected in the lake sediments. Interestingly, the large departure in inclination anomaly around 450–500 A.D. for the SED3k models coincides with a lack of data in that

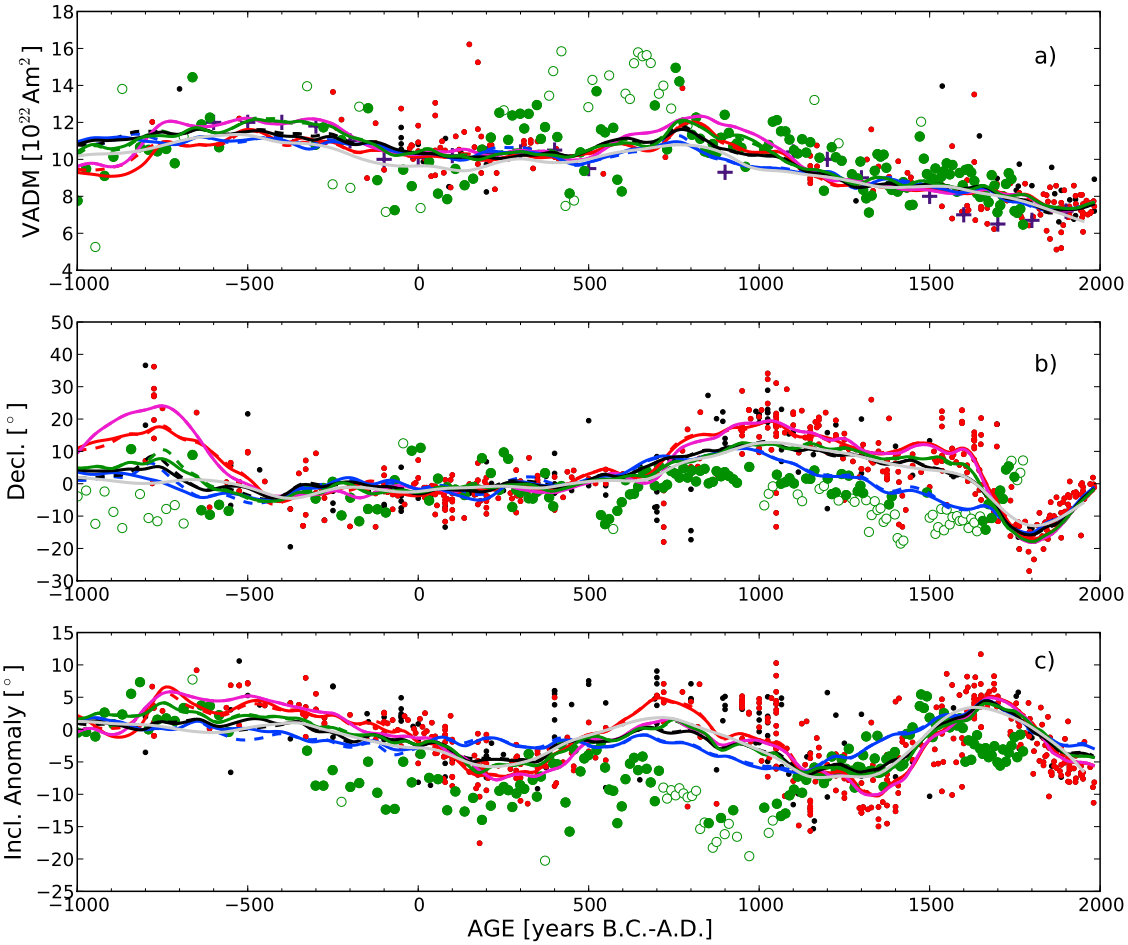

Figure 7. Archeological artifacts within a 1000 km radius around the Mezzano lake in Italy. Observations included in the ARCH3k_cst model are denoted as red circles, and the ones included in the ARCH3k are represented by the additional black circles. Solid green circles denote lake sediments that were selected for the constrained model, and open circles denote those that were rejected. The five pairs of models are colored as follows: ARCH3k (red line), ARCH3kcst (magenta line), SED3k (blue line), CALS3k.3 (black line), and CALS3kcst (green line). Dashed lines represent the version 0 models, and solid lines represent version 1. For comparison, the CALS7K.2 of *Korte and Constable* [2005] is also shown as a gray line. Scaling of the relative intensities was performed taking into account the observations from archeological artifacts. (a) Virtual axial dipole moment versus time and the mixed VDM/VADM curves [*Genevey et al.*, 2008] (purple crosses). (b) Declination versus time and (c) inclination anomaly versus time. Notice how the model fits its own data well in this region abundant with observations.

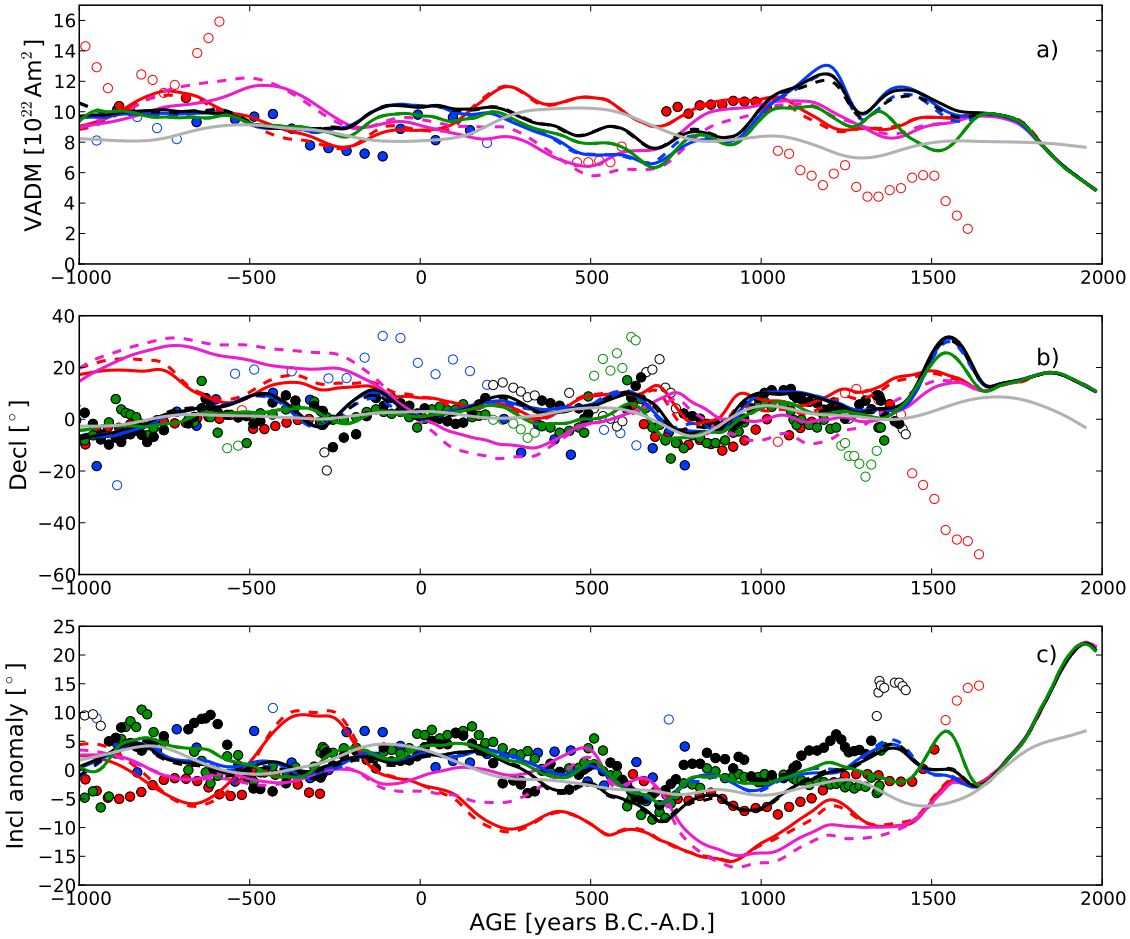

Figure 8. Correlations between the Argentinian lakes: Lake Escondido (ESC, blue circles), Lake Trebol (TRE, red circles), Lake Brazo Campanario (CAM, green circles), and Lake Morenito (MNT, black circles). Data accepted for the constrained model (solid symbols) and rejected data (open symbols) are also shown. The selection criteria remove data when differences between the four different cores are large. The five pairs of models at the location of ESC are colored as follows: ARCH3k (red line), ARCH3kcst (magenta line), SED3k (blue line), CALS3k.3 (black line), and CALS3kcst (green line). Dashed lines represent the version 0 models, and solid lines represent version 1. For comparison, the CALS7K.2 of *Korte and Constable* [2005] is also shown as a gray line. Scaling of the relative intensities was performed taking into account the observations from archeological artifacts or the ARCH3k.0 model (see text). Constraining the data seems to be useful in particular at the youngest end of the core (1400–1600 A.D.), where the end effects becomes visible. (a) Virtual axial dipole moment versus time, (b) declination versus time, and (c) inclination anomaly versus time.

period, a result we would not normally expect from our regularized modeling procedure.

5.2. Residual Analyses

[47] In order to investigate how different data sets fit a particular model, the root mean square (RMS) misfit, normalized to the data uncertainties, were calculated for each data set relative to its own and all other models, using the formula:

$$RMS = \sqrt{\frac{\sum \epsilon_i^2}{N}} \qquad (6)$$

where ϵ_i represents the data residual relative to the model prediction normalized by the uncertainty estimate, and N is the total amount of data. Because the data are not homogeneously distributed in space, we calculated the RMS for the global case (G), the Northern (N), and the Southern Hemisphere case (S). As expected, we have lower RMS residuals in the (comparatively) data rich Northern Hemisphere, whereas in general the Southern Hemisphere shows a worse fit. The results are tabulated in Table 9. We observe that (1) each model best fits the data set from which it is derived; (2) the SED3k_dat1 and CALS3k.3_dat1 data sets have the worst fit to the

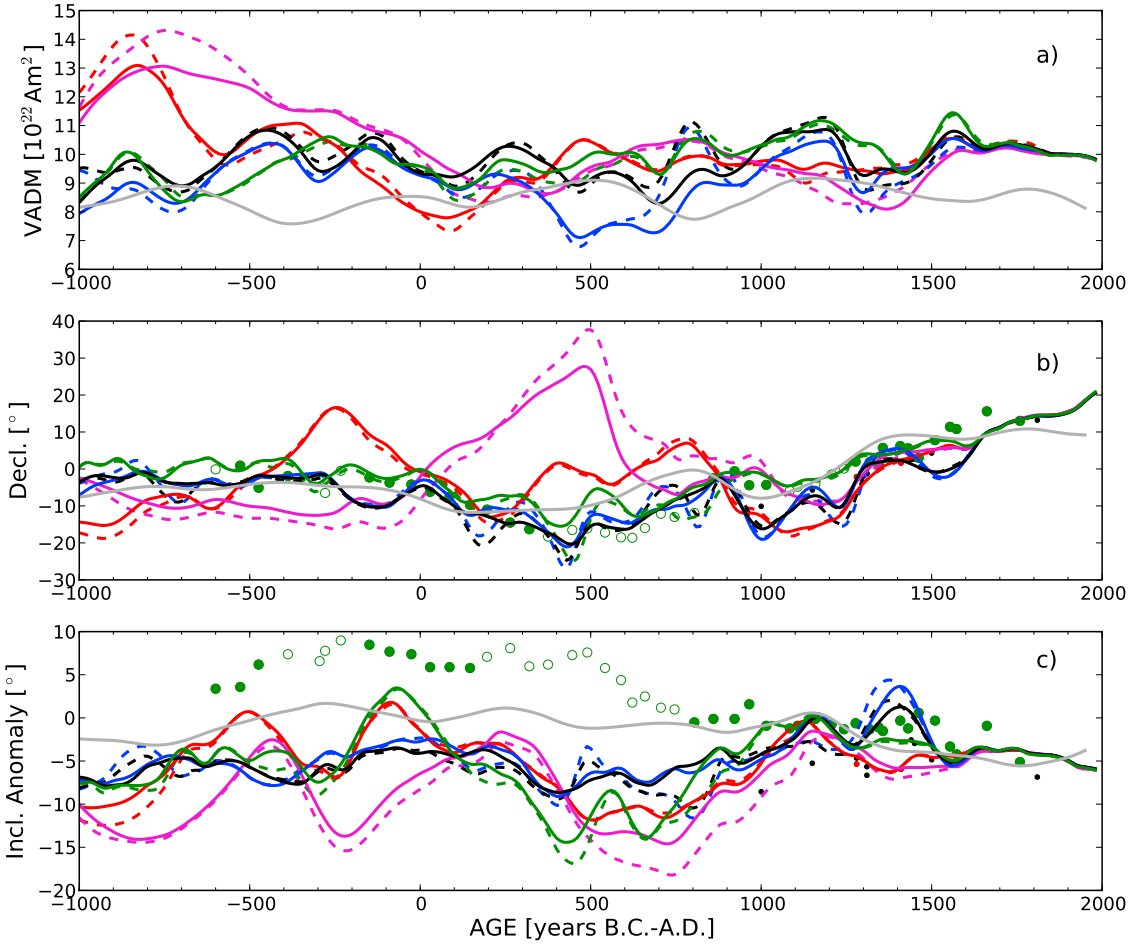

Figure 9. The accepted (rejected) lake sediments data from lake Pounui, New Zealand, shown as green solid (open) circles. This lake is located in an isolated site, and so the selection is based on the ARCH3k.1 model; there are, however, a few directions: the data included in the ARCH3k_cst model are denoted as red circles, and the data included in the ARCH3k are represented by the additional black circles. The five pairs of models are colored as follows: ARCH3k (red line), ARCH3kcst (magenta line), SED3k (blue line), CALS3k.3 (black line), and CALS3kcst (green line). Dashed lines represent the version 0 models, and solid lines represent version 1. For comparison, the CALS7K.2 of *Korte and Constable* [2005] is also shown as a gray line. No relative intensity measurements are available for this lake. Differences between archeological and lake sediments models are more evident for locations where few or no archeological data are available. However, with exception of the constrained archeological model (ARCH3kcst) that shows large departures from the other ones, the trends are similar. (a) Virtual axial dipole moment versus time, (b) declination versus time, and (c) inclination anomaly versus time.

ARCH3k_cst.1 model, which is defined by only 28 data in the Southern Hemisphere; (3) the archeological data sets have the worst fit to the SED3k.1 model; (4) constraining the data sets using data selection leads to smaller misfit; and (5) constrained data sets agree slightly better with the associated unconstrained model than the unconstrained data sets, although the differences are not large.

[48] To check the influence of constrained data selection and statistical rejection of outliers from the data sets, we plot the difference between the predictions of version 1 and constrained version 0 calculated at each site. Figure 12 shows the prediction differences between ARCH3k.1 and ARCH3k_cst.0 in terms of declinations (Figure 12a), inclinations (Figure 12b), and intensities (Figure 12c) during the past 3000 years. Figures 12d–12f present the same differences for the models CALSk3.3 and CALS3k_cst0. The archeological models appear to be reasonably consistent with each other with no major trends over time. There are, however, large differences in intensity around 500 A.D., which arise because the rejection of data significantly reduces the data coverage in every region, especially

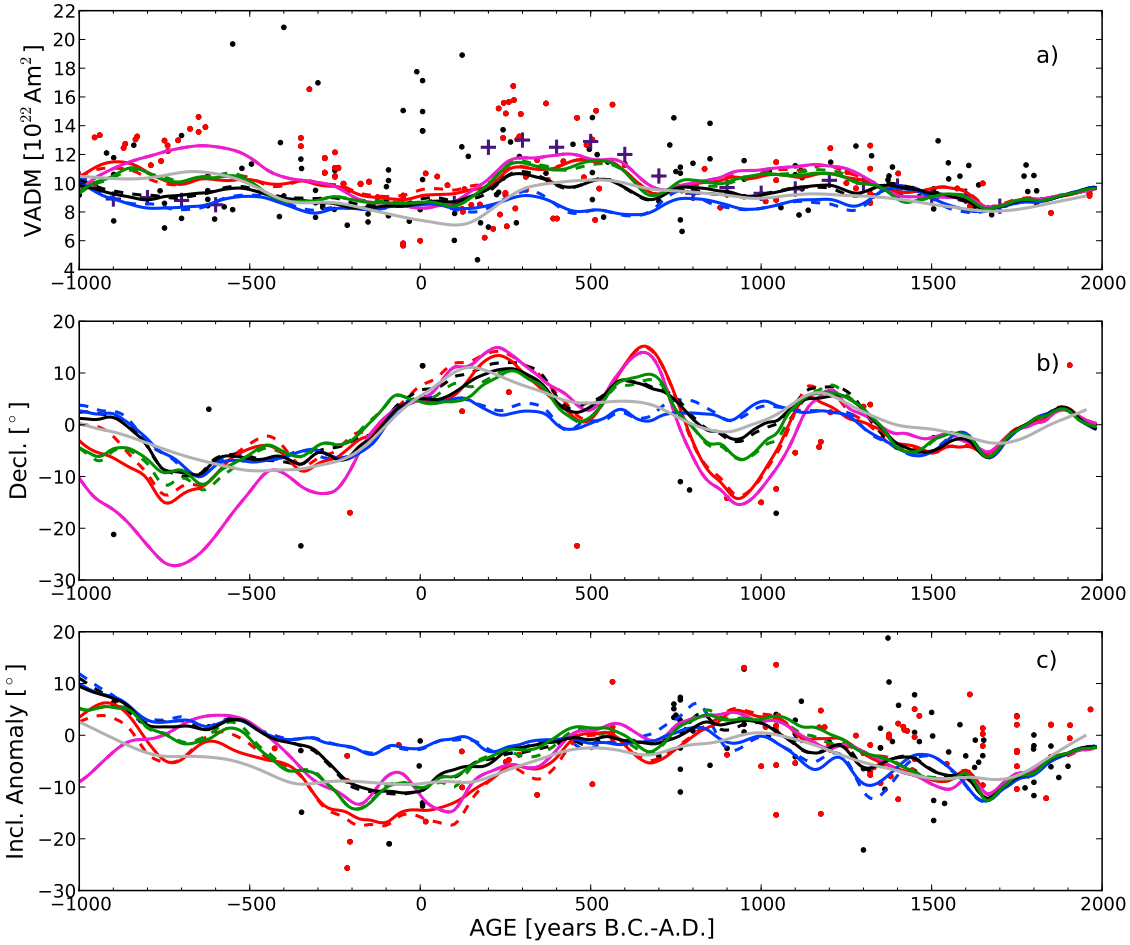

Figure 10. The evolution of the geomagnetic field in east Asia. Observations included in the ARCH3k_cst model are denoted as red circles, and the ones included in the ARCH3k are represented by the additional black circles. The five pairs of models are colored as follows ARCH3k (red line), ARCH3kcst (magenta line), SED3k (blue line), CALS3k.3 (black line), and CALS3kcst (green line). Dashed lines represent the version 0 models, and solid lines represent version 1. For comparison, the CALS7K.2 of *Korte and Constable* [2005] is also shown as a gray line. (a) The VADM of the 10 different models, the archeological artifacts, and the mixed VDM/VADM curves [*Genevey et al.*, 2008] (purple crosses). (b) Declination of the 10 different models compared to the archeological artifacts. (c) Inclination of the models compared to the archeological artifacts.

South America. Large differences in declination predictions occur between 800 and 1700 A.D. for CALS3k.3 versus CALS3k_cst.0, and between 1200 and 1600 A.D. for intensity data.

6. Discussion

[49] The main goal of this study was to achieve the best possible data set for modeling the geomagnetic field over the past 3000 years. We began by compiling all measurements from archeological artifacts and lake sediments. The scaling of the lake sediment relative paleointensities also played an important role allowing the inclusion of new intensity data, especially from the Southern Hemisphere. We then used these data to construct a series of time-varying geomagnetic field models by imposing various constraints on the data selection. As we have already noted, there are different strategies for analyzing the data: for example, *Genevey et al.* [2008] performed a data selection based on quality criteria such as number of data measured and experimental set up; whereas *Korte et al.* [2005] preferred to keep the entire data set and weight individual data according to their uncertainties. There are pros and cons to both strategies, for example, the first approach could lead to biased models if the selections remove a large fraction of the data. Because the data are inhomogeneously distributed, this could have serious implications in areas that are already poor in

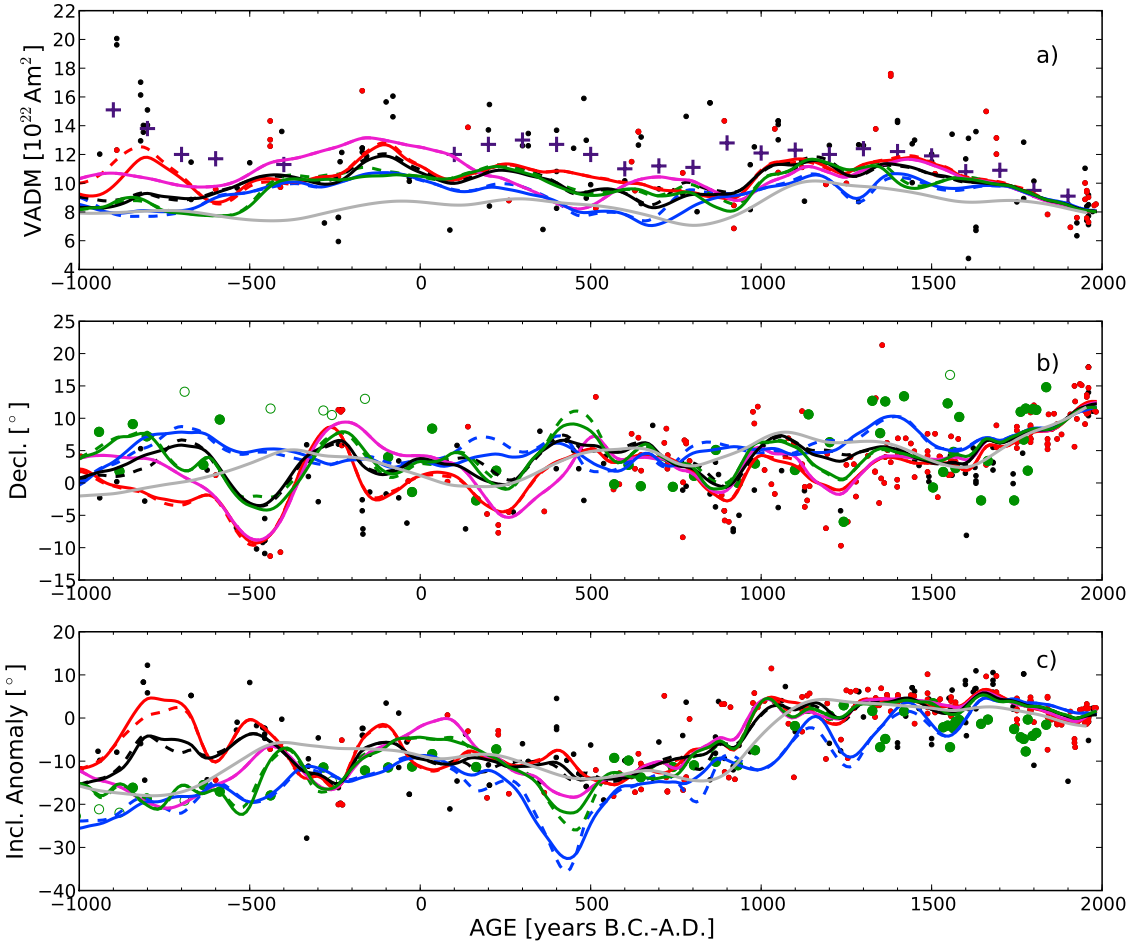

Figure 11. The evolution of the geomagnetic field in Hawaii. Observations included in the ARCH3k_cst model are denoted as red circles, and the ones included in the ARCH3k are represented by the additional black circles. The five pairs of models are colored as follows: ARCH3k (red line), ARCH3kcst (magenta line), SED3k (blue line), CALS3k.3 (black line), and CALS3kcst (green line). Dashed lines represent the version 0 models, and solid lines represent version 1. For comparison, the CALS7K.2 of *Korte and Constable* [2005] is also shown as a gray line. (a) The VADM of the 10 different models, the archeological artifacts, and the mixed VDM/VADM curves [*Genevey et al.*, 2008] (purple crosses). (b) Declination of the 10 different models compared to the archeological artifacts. Lake Waiau (selected) rejected data are shown as (open) solid green circles. (c) Inclination of the models compared to the archeological artifacts and the lake Waiau data.

data (about 80% of the globe). On the other hand, the second approach might be biased by the inclusion of inaccurate observations that contribute significantly to the global analyses, especially if the uncertainties are poorly known. Both effects are likely to be present in the various modeling efforts that we have attempted.

[50] The spatial power spectra for our new suite of models [*Korte et al.*, 2009, Figure 6] indicate that the resolution of the models (by which we mean the amount of spatial and temporal structure) is enhanced compared to CALS7K.2. This is also confirmed by our regional Figures 7–11, which show more detailed temporal variations than CALS7k.2. However, it remains to be demonstrated which of our new models will provide the most accurate predictions of the magnetic field at a given time and place. In fact we have not yet shown that the enhanced resolution corresponds to greater accuracy in the models than for the previous state of the art model, CALS7K.2.

[51] Of course, we expect that in the time interval overlapping with gufm1 the refinements to the modeling technique will result in enhanced accuracy. But the gufm1 penalty also removes one capability for an independent test, in which we regard the

Table 9. Normalized RMS for Each Version 1 Data Set and Model Covering the Past 3000 Years[a]

Data Set	Reg.	N	ARCH3k.1	SED3k.1	CALS3k.3	ARCH3k_cst.1	CALS3k_cst.1
ARCH3k_dat1	G	9843	1.40	2.10	1.59	1.56	1.60
	N	9235	1.40	2.09	1.57	1.53	1.57
	S	248	1.43	2.57	2.05	2.38	2.34
SED3k_dat1	G	20090	2.58	1.89	1.94	2.68	2.09
	N	16135	2.15	1.73	1.79	2.25	1.90
	S	3955	3.87	2.45	2.49	3.98	2.74
CALS3k.3_dat1	G	29585	2.27	1.96	1.83	2.37	1.94
	N	25394	1.92	1.87	1.71	2.02	1.79
	S	4191	3.74	2.42	2.42	3.87	2.68
ARCH3kcst_dat1	G	6122	1.29	1.98	1.46	1.23	1.36
	N	6094	1.29	1.98	1.46	1.23	1.36
	S	28	1.56	1.80	1.69	1.52	1.77
CALS3kcst_dat1	G	19687	1.66	1.54	1.35	1.78	1.27
	N	17472	1.45	1.55	1.33	1.51	1.27
	S	2215	2.80	1.50	1.52	3.18	1.32

[a] Reg. represents the region of interest: global (G), Northern Hemisphere (N), or Southern Hemisphere (S). The number of data for each selection is presented in the column N.

historical field model as the truth and measure our ability to predict it. Still, both our constrained data selection and statistical rejection of outlier strategies show that the global fit of the model to the data improves, and all of our models fit the data better than CALS7K.2.

[52] The overall misfit provides only a general guide to the maximum resolution achievable. The statistics concerning the data and model comparisons clearly indicate that the measurements have significant scatter (in particular in regions with high data density), and the resulting model is a smooth curve that fits between the data. In our attempts to further enhance the resolution of the model, we tried to constrain the data sets by rejecting data with large uncertainties. This does result in a better fit of the model (confirmed by the lower RMS residual in Table 9), but there is no compelling evidence that the resulting model is of higher accuracy or significantly better resolution as we obtain similar power spectra [*Korte et al.*, 2009, Figure 6] for each model.

[53] In discriminating among the new models, we can note that the models created using the constrained data selections (ARCH3k_cst.1 and CALS3k_cst.1) have a considerably lower misfit (Table 9) than the outlier-free models (ARCH3k.1 and CALS3k.1). However, the constrained data selection rejects over 30% of the available data. The constrained rejection of data might be risky in regions poor in measurements, as we observe for the ARCH3k_cst.0 model in South America (Figure 8), for Lake Pounui in New Zealand (Figure 9), and Hawaii (Figure 11). Consequently, we think that the statistical rejection of outliers is the better strategy for a global analysis of the geomagnetic field. We do feel, however, that it might still be appropriate to consider selecting data according to some measures of regional consistency, and this could be particularly useful for sediment data, when several neighboring records can be checked for consistency.

[54] On the other hand, the outlier rejection strategy cannot protect the model against potential bias from data that are inaccurate in some systematic way. For example, we know that the cooling rate correction of paleointensity results is often performed ad libitum, and this might lead to systematic offsets in paleointensity data sets. If such biases can be identified and removed we would be wise to do so. However, the systematic identification of such data remains problematic.

[55] Obviously, the different models best fit their associated data set, and there are significant differences in fit of the models to other data sets. This shows that there are discrepancies among the different recorders, and we think that the appropriate model should be used when comparing the geomagnetic field components of new measurements. In particular, we think that the archeological model ARCH3k.1 is appropriate for geomagnetic field investigations in Europe and Asia: these are the regions where most archeological data are located, and some sediment records seem less consistent with each other and the ARCH3k data; ARCH3k.1 lacks adequate constraints in the Southern Hemisphere as does the constrained archeomagnetic model; CALS3k.3 is more appropriate for investigations on measurements from the rest of the world.

[56] A final point is that when we compare the RMS of the different data sets, we notice that lake

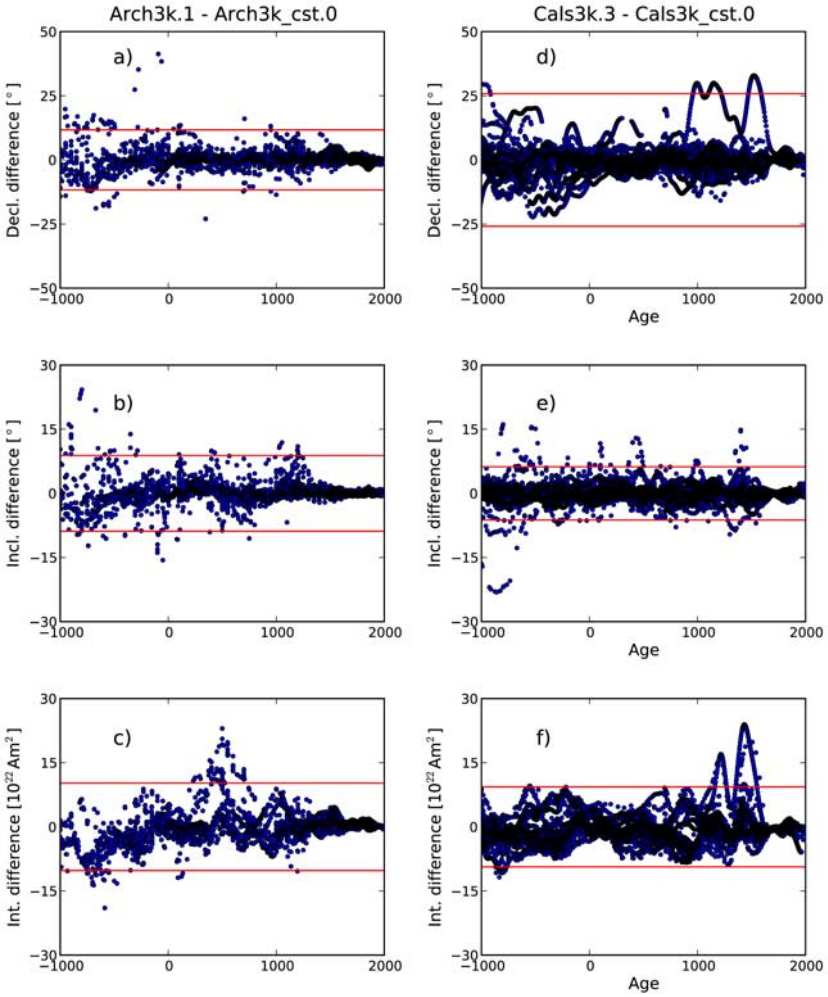

Figure 12. Differences between the predictions between ARCH3k.1 (outlier-free archeological model) and ARCH3k_cst.0 (constrained archeological model) for (a) declinations, (b) inclinations, and (c) intensities. In general the two models agree quite well, apart from significant differences in intensities at around 300–500 A.D. These differences are due to discrepancies in the observations from Central America. (d–f) The same differences between the CALS3k.3 (outlier-free archeological artifacts and lake sediments) and the CALS3k_cst.0 (constrained archeological object and lake sediments) model. In this case the differences show a wider band compared to the archeological artifacts only model, probably due to inconsistencies from neighboring lake sediments. Red lines represent the 3σ bound.

sediments have the largest misfit. This is due to incompatibilities observed among neighboring records. An approach that might be considered in the future is to constrain the lake sediments data set using our a priori selection criteria, merge all the archeological artifacts, and use this mixed data set to create an outlier-free model.

7. Conclusions

[57] The new models presented here are based on updated data sets of archeological and lake sediments magnetic measurements. In particular, compared with its previous version, about 55% of the data used in the CALS3k.3 model are new. The models, although still smooth compared to the actual measurements, have better resolution than CALS7K.2 [*Korte and Constable*, 2005], as based on the spatial power spectra. Constraining the data sets based on data selection appears to be a useful strategy to remove inconsistencies among multiple lake sediment records from a particular area. Otherwise, there is no detectable improvement in model output obtained by data selection constraints, and detrimental effects may result from decreased data coverage. In this sense, we think that the statistical rejection of outliers from a preliminary model is a

more effective and reliable way to avoid inconsistencies. The sediment model SED3k.1 is derived from a data set with better data distribution in time and space than the archeological one; however, the features of the geomagnetic field appear much smoother than for the archeomagnetic model ARCK3k.l. ARCH3k.1 is appropriate for investigating the field evolution in Europe and Asia where there is a comparatively dense distribution of data from archeological artifacts. For a global analysis of the geomagnetic field, we prefer the predictions of CALS3k.3, which is derived from a more homogeneous and complete distribution of data with minimal outlier rejection.

Acknowledgments

[58] This study was supported by NSF grant EAR 0537986 and Academy of Finland grant 119983. We would like to thank several people who provided data: C. Batt, M. Gomez-Paccard, M. Kovacheva, E. Tema, E. Schnepp, and I. Zananiri. We wish to thank Alexandra Lodge for her help in spotting a number of incorrect entries in the GEOMAGIA50 database. We are also most grateful to Roman Leonhardt and two anonymous reviewers for the detailed comments that led us to significantly improve the manuscript.

References

Ali, M., H. Oda, A. Hayashida, K. Takemura, and M. Torii (1999), Holocene palaeomagnetic secular variation at Lake Biwa, central Japan, *Geophys. J. Int.*, *136*, 218–228.

Arai, Y. (1963), Secular variation in intensity of the past geomagnetic field, 84 pp., M.Sc. thesis, Univ. of Tokyo, Tokyo.

Barton, C. E., and M. W. McElhinny (1981), A 10000 yr geomagnetic secular variation record from three Australian maars, *Geophys. J. R. Astron. Soc.*, *67*, 465–485.

Barton, C. E., and T. Torgersen (1988), Palaeomagnetic and ^{210}Pb estimates of sedimentation in Lake Turkana, East Africa, *Palaeogeogr. Palaeoclimatol. Palaeoecol.*, *68*, 53–60.

Bleil, U., and M. Dillon (2008), Holocene Earth's magnetic field variations recorded in marine sediments of the NW African continental margin, *Stud. Geophys. Geod.*, *52*, 133–155.

Bloxham, J., D. Gubbins, and A. Jackson (1989), Geomagnetic secular variation, *Philos. Trans. R. Soc. London*, *329*, 415–502.

Brachfeld, S., and S. K. Banerjee (2000), A new high-resolution geomagnetic relative paleointensity record for the North American Holocene: A comparison of sedimentary and absolute intensity data, *J. Geophys. Res.*, *105*, 821–834.

Brachfeld, S., G. D. Acton, Y. Guyodo, and S. K. Banerjee (2000), High-resolution paleomagnetic records from Holocene sediments from the Palmer Deep, Western Antarctic Peninsula, *Earth Planet. Sci. Lett.*, *181*, 429–441.

Brown, H. (1981), A palaeomagnetic, geochronological and palaeoenvironmental investigation of late and post glacial maar lake sediments from NW Europe, Ph.D. thesis, Univ. of Edinburgh, Edinburgh, U. K.

Burlatskaya, S. P., and Z. A. Chelidze (1990), Geomagnetic field variations in Georgia during the last 15 centuries BC, *Earth Phys.*, *26*, 602–609.

Burlatskaya, S. P., T. Nechaeva, and G. Petrova (1969), Some archeomagnetic data indicative of the westward drift of the geomagnetic field, *Archaeometry*, *11*, 115–130.

Channell, J. E. T., D. A. Hodell, and B. Lehman (1997), Relative geomagnetic paleointensity and δ^{18}O at ODP Site 983 (Gardar Drift, North Atlantic) since 350 ka, *Earth Planet. Sci. Lett.*, *153*, 103–118.

Clark, R. (1975), A calibration curve for radiocarbon dates, *Antiquity*, *49*, 251–266.

Constable, C. (2007), Archeomagnetic and paleomagnetic studies of centennial to millennial-scale geomagnetic field variations, in *Treatise of Geophysics*, vol. 5, *Geomagnetism*, edited by M. Kono and G. Schubert, chap. 9, pp. 337–372, Elsevier, Amsterdam.

Constable, C., and M. Korte (2006), Is Earth's magnetic field reversing?, *Earth Planet. Sci. Lett.*, *246*(1–2), 1–16.

Constable, C. G., and M. W. McElhinny (1985), Holocene geomagnetic secular variation records from north-eastern Australian lake sediments, *Geophys. J. R. Astron. Soc.*, *81*, 103–120.

Cramer, H. (1999), *Mathematical Methods of Statistics*, 575 pp., Princeton Univ. Press, Princeton, N. J.

Creer, K. M., P. W. Readman, and S. Papamarinopoulos (1981), Geomagnetic secular variation in Greece through the last 6000 years obtained from lake sediment studies, *Geophys. J. R. Astron. Soc.*, *66*, 147–193.

Creer, K. M., D. A. Valencio, A. M. Sinito, P. Tucholka, and J. F. Vilas (1983), Geomagnetic secular variation 0–14000 yr BP as recorded by lake sediments from Argentina, *Geophys. J. R. Astron. Soc.*, *74*, 199–221.

Donadini, F., and L. Pesonen (2007), Archeointensity determinations from Finland, Estonia, and Italy, *Geophysica*, *43*(1–2), 3–18.

Donadini, F., K. Korhonen, P. Riisager, and L. Pesonen (2006), Database for Holocene geomagnetic intensity information, *Eos Trans. AGU*, *87*(14), 137.

Donadini, F., P. Riisager, K. Korhonen, K. Kahma, L. Pesonen, and I. Snowball (2007), Holocene geomagnetic paleointensities: A blind test of absolute paleointensity techniques and materials, *Phys. Earth Planet. Inter.*, *161*, 19–35.

Dumberry, M., and C. C. Finlay (2007), Eastward and westward drift of the Earth's magnetic field for the last three millennia, *Earth Planet. Sci. Lett.*, *254*, 146–157.

Eighmy, J. L., and R. S. Sternberg (1990), *Archeomagnetic Dating*, 450 pp., Univ. of Ariz. Press, Tucson.

Frank, U., N. R. Nowaczyk, J. F. W. Negendank, and M. Melles (2002a), A paleomagnetic record from Lake Lama, northern central Siberia, *Phys. Earth Planet. Inter.*, *133*, 3–20.

Frank, U., M. J. Schwab, and J. F. W. Negendank (2002b), A lacustrine record of paleomagnetic secular variation from Birkat Ram, Golan Heights, (Israel) for the last 4400 years, *Phys. Earth Planet. Inter.*, *133*, 21–34.

Frank, U., M. J. Schwab, and J. F. W. Negendank (2003), Results of rock magnetic investigations and relative paleointensity determinations on lacustrine sediments from Birkat Ram, Golan Heights (Israel), *J. Geophys. Res.*, *108*(B8), 2379, doi:10.1029/2002JB002049.

Frank, U., N. Nowaczyk, and J. Negendank (2007), Palaeomagnetism of greigite bearing sediments from the Dead Sea, Israel, *Geophys. J. Int.*, *168*, 904–920.

Gallet, Y., A. Genevey, and V. Courtillot (2003), On the possible occurrence of archeomagnetic jerks in the geomagnetic field over the past three millenia, *Earth Planet. Sci. Lett.*, *214*, 237–252.

Genevey, A., Y. Gallet, C. G. Constable, M. Korte, and G. Hulot (2008), ArcheoInt: An upgraded compilation of geomagnetic

field intensity data for the past ten millennia and its application to the recovery of the past dipole moment, *Geochem. Geophys. Geosyst.*, *9*, Q04038, doi:10.1029/2007GC001881.
Gogorza, C., A. Sinito, J. Lirio, H. Nuñez, M. Chaparro, and J. Vilas (2002), Paleosecular variations 0–19000 years recorded by sediments from Escondido Lake (Argentina), *Phys. Earth Planet. Inter.*, *133*, 35–55.
Gogorza, C. S. G., J. M. Lirio, H. Nuñez, M. Chaparro, H. R. Bertorello, and A. M. Sinito (2004), Paleointensity studies on Holocene-Pleistocene sediments from Lake Escondido, Argentina, *Phys. Earth Planet. Inter.*, *145*, 219–238.
Gogorza, C., M. Irurzun, M. Chaparro, J. Lirio, H. Nunez, P. Becoff, and A. Sinito (2006), Relative paleointensity of the geomagnetic field over the last 21000 years BP from sediment cores, Lake El Trébol (Patagonia, Argentina), *Earth Planets Space*, *58*, 1323–1332.
Gomez-Paccard, M., A. Chauvin, P. Lanos, J. Thiriot, and P. Jimenez-Castillo (2006), Archeomagnetic study of seven contemporaneous kilns from Murcia (Spain), *Phys. Earth Planet. Inter.*, *157*, 16–32.
Hogg, E. (1978), The Holocene geomagnetic field in Europe, Ph.D. thesis, Univ. of Edinburgh, Edinburgh, U. K.
Hulot, G., C. Eymin, B. Langlais, M. Mandea, and N. Olsen (2002), Small-scale structure of the geodynamo inferred from Oersted and Magsat satellite data, *Nature*, *416*, 620–623.
Huttunen, P., and J. Stober (1980), Dating of palaeomagnetic records from Finnish lake sediment cores using pollen analysis, *Boreas*, *9*, 193–202.
Irurzun, M., C. Gogorza, M. Chaparro, J. Lirio, H. Nuñez, J. Vilas, and A. Sinito (2006), Paleosecular variations recorded by Holocene-Pleistocene sediments from Lake El Trébol (Patagonia, Argentina), *Phys. Earth Planet. Inter.*, *154*, 1–17.
Jackson, A., A. Jonkers, and M. Walker (2000), Four centuries of geomagnetic secular variation from historical records, *Philos. Trans. R. Soc. London, Ser. A*, *358*, 957–990.
King, J. K. (1983), Geomagnetic secular variation curves for northeastern North America for the last 9000 years, Ph.D. thesis, Univ. of Minn., Minneapolis.
Korhonen, K., F. Donadini, P. Riisager, and L. J. Pesonen (2008), GEOMAGIA50: An archeointensity database with PHP and MySQL, *Geochem. Geophys. Geosyst.*, *9*, Q04029, doi:10.1029/2007GC001893.
Korte, M., and C. Constable (2003), Continuous global geomagnetic field models for the past 3000 years, *Phys. Earth Planet. Inter.*, *140*, 73–89.
Korte, M., and C. Constable (2005), The geomagnetic dipole moment over the last 7000 years—New results from a global model, *Earth Planet. Sci. Lett.*, *236*, 348–358.
Korte, M., and C. G. Constable (2006a), On the use of calibrated relative paleointensity records to improve millennial-scale geomagnetic field models, *Geochem. Geophys. Geosyst.*, *7*, Q09004, doi:10.1029/2006GC001368.
Korte, M., and C. Constable (2006b), Spatial and temporal resolution of millenial scale geomagnetic field models, *Adv. Space Res.*, *7*, 57–69, doi:10.1016/j.asr.2007.03.094.
Korte, M., A. Genevey, C. G. Constable, U. Frank, and E. Schnepp (2005), Continuous geomagnetic field models for the past 7 millennia: 1. A new global data compilation, *Geochem. Geophys. Geosyst.*, *6*, Q02H15, doi:10.1029/2004GC000800.
Korte, M., F. Donadini, and C. Constable (2009), Geomagnetic field for 0–3 ka: 2. Revised global time-varying models, *Geochem. Geophys. Geosyst.*, *10*, Q06008, doi:10.1029/2008GC002297.
Kovacheva, M. (1997), Archaeomagnetic database from Bulgaria: The last 8000 years, *Phys. Earth Planet. Inter.*, *102*, 145–151.
Kovacheva, M., Y. Boyadziev, M. Kostadinova, N. Jordanova, and F. Donadini (2009), Updated archeomagnetic data set of the past 8 millennia from the Sofia laboratory, Bulgaria, *Geochem. Geophys. Geosyst.*, *10*, Q05002, doi:10.1029/2008GC002347.
Lanos, P., M. LeGoff, M. Kovacheva, and E. Schnepp (2005), Hierarchical modelling of archaeomagnetic data and curve estimation by moving average technique, *Geophys. J. Int.*, *160*, 440–476.
Lanza, R., A. Meloni, and E. Tema (2005), Historical measurements of the Earth's magnetic field compared with remanence directions from lava flows in Italy over the last four centuries, *Phys. Earth Planet. Inter.*, *148*, 97–107.
Lodge, A., and R. Holme (2008), Towards a new approach to archeomagnetic dating in Europe using geomagnetic field modeling, *Archaeometry*, *50*, 309–322, doi:10.1111/j.1475-4754.2008.00400.x.
Lund, S. P., and S. K. Banerjee (1985), Late Quaternary paleomagnetic field secular variation from two Minnesota lakes, *J. Geophys. Res.*, *90*, 803–825.
Márton, P., and E. Ferencz (2006), Hierarchical versus stratification statistical analysis of archeomagnetic directions: The secular variation curve for Hungary, *Geophys. J. Int.*, *164*, 484–494.
Merrill, R., M.-W. McElhinny, and M. McFadden (1996), *The Magnetic Field of the Earth*, 531 pp., Academic, San Diego, Calif.
Mothersill, J. S. (1979), The palaeomagnetic record of the late Quaternary sediments of Thunder Bay, *Can. J. Earth Sci.*, *16*, 1016–1023.
Mothersill, J. S. (1981), Late Quaternary palaeomagnetic record of the Goderich Basin, Lake Huron, *Can. J. Earth Sci.*, *18*, 448–456.
Mothersill, J. S. (1996), Paleomagnetic results from lakes Victoria and Albert, Uganda, *Stud. Geophys. Geod.*, *40*, 25–35.
Nourgaliev, D. K., A. S. Borisov, F. Heller, B. V. Burov, P. G. Jasonov, D. I. Khasanov, and S. Z. Ibragimov (1996), Geomagnetic secular variation through the last 3500 years as recorded by Lake Aslikul sediments from eastern Europe (Russia), *Geophys. Res. Lett.*, *23*, 375–378.
Nourgaliev, D. K., F. Heller, A. S. Borisov, I. Hajdas, G. Bonani, P. G. Iassonov, and H. Oberhänsli (2003), Very high resolution paleosecular variation record for the last ~1200 years from the Aral Sea, *Geophys. Res. Lett.*, *30*(17), 1914, doi:10. 1029/2003GL018145.
Nourgaliev, D., F. Heller, A. Borisov, P. Yasonov, I. Chernova, and I. Hajdas (2005), Principal features (master curve) of geomagnetic field variations in Belorussia during the last 12 thousand years, *Russ. J. Earth Sci.*, *7*, 1–16.
Ojala, A., and T. Saarinen (2002), Paleosecular variation of the Earth's magnetic field during the last 10000 years based on an annually laminated sediment of Lake Nautajärvi, central Finland, *Holocene*, *12*, 391–400.
Ojala, A., and M. Tiljander (2003), Testing the fidelity of sediment chronology: Comparison of varve and paleomagnetic results from Holocene lake sediments from central Finland, *Quat. Sci. Rev.*, *22*, 1787–1803.
Pavon-Carrasco, J., M. Osete, M. Torta, and L. R. Gaya-Piqué (2008), A regional archaeomagnetic model for the palaeointensity in Europe for the last 2000 years and its implications for climatic change, *Pure Appl. Geophys.*, *165*, 1209–1225.
Peck, J. A., J. W. King, S. M. Colman, and V. A. Kravchinsky (1996), An 84-kyr paleomagnetic record from the sediments of Lake Baikal, Siberia, *J. Geophys. Res.*, *101*, 11,365–11,385.
Peng, L., and J. W. King (1992), A late Quaternary geomagnetic secular variation record from Lake Waiau, Hawaii, and

the question of the Pacific nondipole low, *J. Geophys. Res.*, *97*, 4407–4424.
Piper, J. D. A. (1989), Palaeomagnetism, in *Geomagnetism*, vol. 3, edited by J. A. Jacobs, Academic, London.
Ramsey, B. (1994), Analysis of chronological information and radiocarbon calibration: The program OxCal, *Archaeol. Comput. Newsl.*, *41*, 11–16.
Reimer, P., et al. (2004), IntCal04 Terrestrial radiocarbon age calibration, 26–0 ka BP, *Radiocarbon*, *46*, 1029–1058.
Saarinen, T. (1998), High-resolution palaeosecular variation in northern Europe during the last 3200 years, *Phys. Earth Planet. Inter.*, *106*, 299–309.
Schnepp, E., and P. Lanos (2006), A preliminary secular variation reference curve for archaeomagnetic dating in Austria, *Geophys. J. Int.*, *166*, 91–96.
Snowball, I., and P. Sandgren (2002), Geomagnetic field variations in northern Sweden during the Holocene quantified from varved lake sediments and their implications for cosmogenic nuclide production rates, *Holocene*, *12*, 517–530.
Snowball, I., L. Zillen, A. Ojala, T. Saarinen, and P. Sandgren (2007), FENNOSTACK and FENNOPRIS: Varve dated Holocene palaeomagnetic secular variation and relative palaeointensity stacks for Fennoscandia, *Earth Planet. Sci. Lett.*, *255*, 106–116.
Stoner, J., A. Jennings, G. Kristjánsdóttir, G. Dunhill, J. Andrews, and J. Hardardóttir (2007), A paleomagnetic approach toward refining Holocene radiocarbon-based chronologies: Paleoceanographic records from the north Iceland (MD99-2269) and east Greenland (MD99-2322) margins, *Paleoceanography*, *22*, PA1209, doi:10.1029/2006PA001285.
St-Onge, G., J. Stoner, and C. Hillaire-Marcel (2003), Holocene paleomagnetic records from the St. Lawrence Estuary, eastern Canada: Centennial- to millennial-scale geomagnetic modulation of cosmogenic isotopes, *Earth Planet. Sci. Lett.*, *209*, 113–130.
Stuiver, M., and P. J. Reimer (1993), Extended ^{14}C data base and revised CALIB 3.0 ^{14}C age calibration program, *Radiocarbon*, *35*, 215–230.
Tauxe, L. (1993), Sedimentary records of relative paleointensity of the geomagnetic field: Theory and practice, *Rev. Geophys.*, *31*, 319–354.
Tauxe, L., J. Steindorf, and A. Harris (2006), Depositional remanent magnetization: Toward an improved theoretical and experimental foundation, *Earth Planet. Sci. Lett.*, *244*, 515–529.
Tema, E., I. Hedley, and P. Lanos (2006), Archaeomagnetism in Italy: A compilation of data including new results and a preliminary Italian secular variation curve, *Geophys. J. Int.*, *167*, 1160–1171.
Thomson, R., and G. M. Turner (1985), Icelandic Holocene palaeomagnetism, *Phys. Earth Planet. Inter.*, *38*, 250–261.
Thouveny, N., and D. Williamson (1988), Paleomagnetic study of the Holocene and upper Pleistocene sediments from lake Barombi Mbo. Cameroun: First results, *Phys. Earth Planet. Inter.*, *52*, 193–206.
Turner, G. M. (1987), A 5000 year geomagnetic palaeosecular variation record from western Canada, *Geophys. J. R. Astron. Soc.*, *91*, 103–121.
Turner, G. M., and D. A. Lillis (1994), A palaeomagnetic secular variation record for New Zealand during the past 2500 years, *Phys. Earth Planet. Inter.*, *83*, 265–282.
Turner, G. M., and R. Thomson (1979), Behaviour of the Earth's magnetic field as recorded in the sediment of Loch Lomond, *Earth Planet. Sci. Lett.*, *42*, 412–426.
Turner, G. M., and R. Thomson (1981), Lake sediment record of the geomagnetic secular variation in Britain during Holocene times, *Geophys. J. R. Astron. Soc.*, *65*, 703–725.
Valet, J.-P. (2003), Time variations in geomagnetic intensity, *Rev. Geophys.*, *41*(1), 1004, doi:10.1029/2001RG000104.
Verosub, K. L., P. J. Mehringer, and P. Waterstraat (1986), Holocene secular variation in western North America: Paleomagnetic record from Fish Lake, Harney County, Oregon, *J. Geophys. Res.*, *91*, 3609–3623.
Vigliotti, L. (2006), Secular variation record of the Earth's magnetic field in Italy during the Holocene: Constraints for the construction of a master curve, *Geophys. J. Int.*, *165*, 414–429.
Wardinski, I., and M. Korte (2008), The evolution of the core-surface flow over the last seven thousand years, *J. Geophys. Res.*, *113*, B05101, doi:10.1029/2007JB005024.
Zananiri, I., C. Batt, P. Lanos, D. Tarling, and P. Linford (2007), Archeomagnetic secular variation in the UK during the past 4000 years and its application to archeomagnetic dating, *Phys. Earth Planet. Inter.*, *167*, 97–107.
Zhu, R., Z. Gu, B. Huang, Z. Jin, X. Wei, and C. Li (1994), Geomagnetic secular variations and climate changes since 15,000 a B.P., Beijing region, *Sci. Sin.*, *37*, 984–990.
Zillén, L. (2003), Setting the Holocene clock using varved lake sediments in Sweden, Ph.D. thesis, Quat. Sci., Dep. of Geol., Lund Univ., Lund, Sweden.